RSC Advances

ROYAL SOCIETY OF CHEMISTRY

www.rsc.org/advances

Graphical Abstract

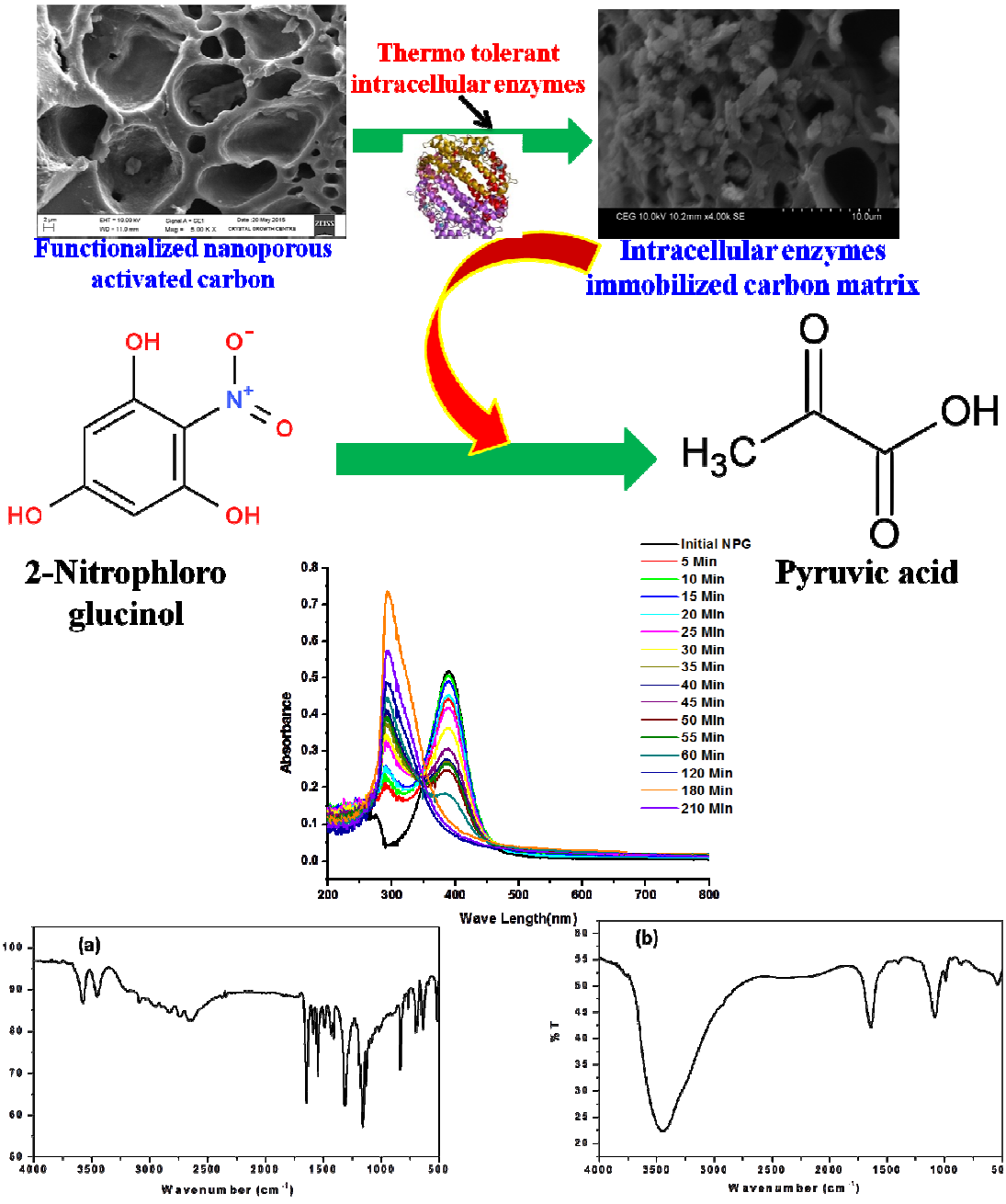

Immobilization of thermo tolerant intracellular enzymes on functionalized Nanoporous activated carbon and its application on degradation of an endocrine disruptor: Kinetic, Isotherm and thermodynamics studies

P. Saranya, S.Ranjitha & G.Sekaran*

Environmental Technology Division, CSIR-Central Leather Research Institute (CLRI), Adyar, Chennai, India

Corresponding Author:

Tel: +91-44-24452941

Fax: +91-44-24410232

E-mail address: ganesansekaran@gmail.com (Dr.G.Sekaran)

Abstract

A bacterium, *Serratia marcescens* capable of degrading the endocrine disruptor, 2-Nitrophloroglucinol (NPG) was isolated from the tannery wastewater contaminated soil. The mixed intracellular enzymes (MICE) produced from *S. marcescens* were extracted and characterized. The functionalized Nanoporous activated carbon matrix (FNAC) was prepared to immobilize MICE. The optimum conditions for the immobilization of MICE on FNAC were found to be time, 2.5 h; pH, 7.0; temperature, 40ºC; concentration of MICE, 4mg; particle size of FNAC, 300µm and mass of FNAC, 1 g. The FNAC before and after immobilization of MICE were characterized using Scanning electron microscopy, Fourier Transform-Infrared Spectrophotometer and X-ray diffractometer. The thermal behaviour of the free and the immobilized MICE was studied using Thermogravimetric analysis. The immobilization of MICE on FNAC obeyed Freundlich model and the immobilization process followed pseudo second order kinetic model. MICE-FNAC matrix was used to degrade NPG in aqueous solution. The degradation of NPG by MICE-FNAC was optimum at contact time, 3 h; pH, 7.0; temperature, 40 ºC; concentration of NPG, 20 µM and agitation speed, 70 rpm. The degradation of NPG was found to be enhanced in the presence of Zn^{2+}, Cu^{2+}, Ca^{2+} and V^{3+} ions. The degradation of NPG by MICE-FNAC was studied using UV-Visible, fluorescence and FTIR spectroscopy. The degradation of NPG by MICE-FNAC was confirmed using HPLC, NMR and GC-MS spectroscopy.

Keywords: Nitro phloroglucinol, *Serratia marcescens*, mixed intracellular enzymes, Immobilization, functionalized Nanoporous activated carbon.

1. Introduction

Endocrine disrupting compounds are the group of environmental pollutants mimicking natural hormones, disruption of biosignal pathways or modification of hormone receptors.[1] The endocrine disrupting chemicals have received increased attention in water quality management and healthcare management due to their persistence in the environment and toxic activity even at low concentration.[2]

Nitro phloroglucinol (NPG) has been widely used in chemical industry as a raw material for manufacturing dye and in explosive industry as an ingredient for priming composition, percussion caps and detonator formulations.[3, 4] NPG is a synthetic intermediate in the manufacture of benzoxazoles and benzothiazoles as selective ligands for human β-estrogen receptor (ER- β)[5] and thus it has the ability to bind with the estrogen receptor. In leather industry, use of soluble dyes such as sulphur black 1, sulphur brown 14, sulphur red 6 and other sulphur based dyes could be the source for the presence of NPG in tannery wastewater. NPG is characterized by density (1.771 g cm^{-3}), boiling point (343°C), and melting point (189 – 193 ºC).

Nitroaromatic compounds are among the largest and most important groups of industrial chemicals in use. The ability of the nitro group to delocalize π electrons of the phenyl ring to satisfy its own charge deficiency and impart charge to the molecule. The nitro group is strongly deactivated towards electrophilic aromatic substitution of the benzene ring.[6]

The stability and recalcitrant nature of NPG are due to both the conjugation state and resonance properties of nitro groups attached to aromatic rings.[6] The conventional biological treatment of nitro compounds has certain disadvantages such as high sludge production, high energy demand and frequent maintenance requirement[7] besides large land area requirement and less flexibility in design & operation.[8] Other methods such as adsorption, photolysis, chemical

oxidation and electrochemical technique, are widely used for the treatment of nitro compounds containing wastewater. [9] However, all these methods have their own limitations in the field level implementation due to high capital cost, large area requirement and high electrical energy demand.[9]

Advanced oxidation processes (AOPs), based on the in situ generation of non selective and highly reactive species such as hydroxyl radicals (•OH), superoxide anion radicals (O_2•−), and hydrogen peroxide (H_2O_2) as initiators of the oxidative degradation of refractory organics, have been proposed as an alternative approach to the conventional methods in recent years.[10] AOP with ozone (O_3), ultraviolet (UV), hydrogen peroxide (H_2O_2) and/or catalyst offered a powerful water treatment solution for the reduction and/or removal of refractory organic compounds.[11-13] The main disadvantages of AOP are high operation costs due to chemicals and/or energy input, formation of oxidation intermediates potentially toxic and complicated design procedures.[14]

The biodegradation of pollutants in wastewater mainly depends on microorganisms that attack the pollutants enzymatically and convert them into nonhazardous products. [15] Bacteria that inhabit chemical waste contaminated sites possess an astonishing ability of evolving new pathways for catabolism of recalcitrant organic compounds. Such pathways are accompanied by the appearance of transcriptional regulatory circuits that adjust the level of biodegradative capacity of the bacteria. Transcriptional regulation mediated by the binding of organic effector on a regulatory protein that acts on specific protein seems to be late evolutionary development as compared to metabolic operons and enzymes.[16] Biodegradation of aromatic compounds has therefore, gained an increasing attention in pollution prevention. [17, 18]

In biodegradation of wastewater, toxic pollutants were eliminated either through intracellular accumulation or through enzymatic transformation into less/nontoxic compounds, [19] applicable only to labile organic compounds. Sometimes the secondary metabolites of the pollutants are more toxic and persistent than the parent compounds.[20] Hence, there has been constant research on the development of cost effective techniques for the treatment of nitro organic compounds in wastewater. The removal of aromatic nitro groups by dioxygenase was first reported by Ecker *et al*.[21] Additional support for the reaction mechanism came from the observation recorded by Sander *et al.* [22] that the enzyme from a *Pseudomonas sp.* could catalyze the elimination of the nitro group from 2, 4, 5-trichloronitrobenzene.

The intracellular enzymes were explored for wastewater treatment as they were highly specific and extremely efficient catalysts[23] and could degrade the target pollutant. The general disadvantages observed with the application of free enzymes for the bioremediation of wastewater containing refractory organic compounds were periodic addition increased the operation cost, applied free enzyme increased COD load, and sometimes enzyme activity was lost due to the fluctuating environmental conditions. Hence, immobilization technology has been widely used for improving the activity, stability, specificity, selectivity and decreased inhibition of enzymes. [24, 25] The function of an intracellular enzyme depends largely on its conformation geometry. The stereo chemical configuration of an intracellular enzyme changes with harsh conditions such as high temperature, very low/high pH, high concentration of target pollutants and high ionic strength.[26] The immobilized enzyme in its physical confinement to a certain region of space, retained its catalytic activity with the capacity to be used continuously.[27] Few research studies have employed certain support matrices such as epoxy activated matrix, sepabeads, curdlan matrix for the enzyme immobilization.[28] The immobilization of enzymes on

activated carbon was observed to be nontoxic, fast, inexpensive, easy to handle and stable against denaturation by oxidants.[29] However, there is no single report on the immobilization of intracellular enzymes and thereof for the degradation of NPG in wastewater. Hence, in the present investigation, mixed intracellular enzymes (MICE) were extracted from *Serratia marcescens* and characterized. MICE was immobilized on functionalized Nanoporous activated carbon (FNAC) and used for the degradation of NPG. The kinetics and thermodynamics for the immobilization of MICE on FNAC have been evaluated.

2. Materials and Methods

2.1. Material

2-Nitrophloroglucinol of high purity 98% was obtained from Alfa Aesar (India). Ethylenediamine and glutaraldehyde of purity 99.5% were purchased from Sigma–Aldrich–Fluka Chemical Co., India.

2.2. Culture enrichment and isolation

The NPG degrading bacterium was isolated from the terrestrial soil acclimatized with NPG. Enrichment was carried out in M9 Minimal media (HiMedia) of volume 100 mL with samples containing 150 µM of NPG as the sole carbon source. NPG concentration in minimal media was increased from 30 to 150 µM with an incremental increase of 5 µM. A pigmented bacterium isolated from the acclimatized soil was observed to degrade NPG in the solution.

2.3. Identification of the strains and phylogenic analysis

The pigmented bacterium was identified by 16S ribosomal DNA (16S rDNA) sequencing and phylogenetic analysis. The genomic DNA was isolated according to the procedure of Marmur.[30] Phylogenetic analysis was performed by subjecting the deduced sequence to the 16S

rDNA database to obtain the similar sequences and the phylogenetic tree was constructed using the Phylip package.[31]

2.4 Culture conditions for intracellular enzyme production

The bacterium was aseptically inoculated into Erlenmeyer flasks of volume 1000 ml containing 75 µM NPG as the substrate in 500 ml of minimal media of pH 7 for intracellular enzyme production. The culture flasks were incubated on the shaker at 150 rpm and at 35ºC for 72h. The bacterial cells were separated from the culture flasks by centrifugation at 6000 rpm for 20 min. The bacterial biomass was washed twice with phosphate buffer (pH 7.0) and stored at -20º C.

2.5 Extraction of intracellular enzymes

The method for intracellular protein extraction was adapted from Naiem and Jai[32] with some modifications. The bacterial cells were sonicated with 1 ml of 0.1 M phosphate buffer. The extracts were centrifuged at 14,000×g for 30 min. The cell-free supernatant was collected and dialyzed against 0.1 M phosphate buffer (pH 7.0) for overnight. The purified mixed intracellular enzymes (MICE) were lyophilized and used for further analysis and for the degradation of NPG.

2.6 Assays of intracellular enzymes

The lyophilized enzyme was analyzed for various intracellular enzymes present. The enzymes involved in the degradation of NPG were determined using the respective assay procedures: Catechol dioxygenase,[33] Dehydrogenase,[34] Phenol hydroxylase,[35] Alkaline phosphatase,[36] Pyruvate decarboxylase,[37] Nitrate reductase[38] and Pyruvate kinase.[39] The concentration of intracellular enzymes were expressed in terms of protein content, following Lowry method[40], employing bovine serum albumin as the standard. The intracellular enzymes were quantified and used as a mixture of intracellular enzymes for the degradation of NPG.

158 **2.7 Molecular weight determination of Purified intracellular enzymes**

159 The molecular weight of enzymes was determined by using sodium dodecyl sulphate -
160 polyacrylamide gel electrophoresis (SDS-PAGE) according to the method followed by
161 Lammeli,[41] on a 5 % stacking gel and 12 % resolving gel. The protein marker ranging from 5 to
162 240 KDa was used as a standard marker for determination of molecular weight.

163 **2.8 Aminoacid composition of MICE by HPLC**

164 The MICE was hydrolyzed at 100 ºC for 24 h with 6 N HCl and neutralized with 1N
165 NaOH. The amino acid composition was analyzed using Agilent 1100 HPLC amino acid
166 analyzer, and the data analysis was performed by using HP chem station.

167 **2.9 Preparation of functionalized Nanoporous activated carbon (FNAC)**

168 Nanoporous activated carbon (NAC) was prepared from rice husk and the
169 functionalization of the NAC was carried out as explained by Ramani *et al*.[42] The washed FNAC
170 was dried at 110°C for 6 h and it was sieved to different sizes as 100, 300, 400 and 600 µm.

171 **2.10. Immobilization of MICE on FNAC**

172 The optimum conditions for the immobilization of MICE on FNAC were determined by
173 varying the parameters such as time (30 to 210 min), pH (1.0 - 10.0), temperature (20 to 60ºC),
174 concentration of MICE (1- 5 mg), particle size of FNAC (100, 300, 400 & 600µm) and mass of
175 FNAC (0.5- 2.5 g). The immobilization of MICE was carried out by equilibrating 1 g of FNAC
176 with phosphate buffer of volume 15 ml at pH 7 containing a known amount of lyophilized
177 MICE. A mg of lyophilized MICE contains 532.9 mg of protein. Immobilization capacity was
178 measured in terms of residual protein content as shown by the mathematical expression.

$$Immobilization\ capacity\ \left(\frac{mg}{g}\right) = \frac{Initial\ concentration\ of\ MICE\ (as\ protein) - Final\ concentration\ of\ MICE}{Mass\ of\ FNAC\left(1 - \frac{moisture\ content}{100}\right)} \quad (1)$$

2.10.1. Nonlinear kinetic model for the immobilization of MICE on FNAC

In order to investigate the kinetic rate constants for the immobilization of MICE on FNAC, the pseudo first order[43] and pseudo second order[44] kinetic models were employed, following the equations (eqn 2 and 3), respectively.

$$q_t = q_e\ (1 - exp^{-k_1\ t}) \quad (2)$$

$$q_t = \frac{k_2 q_e^2 t}{1 + k_2 q_e t} \quad (3)$$

where q_e and q_t are the amounts of MICE immobilized (mg/g of FNAC) at equilibrium and at time (t) respectively, k_1 and k_2 are the first and second order rate constants.

2.10.2. Thermodynamic studies on immobilization of MICE on FNAC

The classical Van't Hoff equation was used to determine the thermodynamic properties such as change in Gibbs free energy (ΔG^o), entropy (ΔS^o) and enthalpy (ΔH^o) for the immobilization of MICE on FNAC.

$$\Delta G^o = \Delta H^o - T\Delta S^o \quad (4)$$

2.11. Instrumental techniques for evaluation of immobilization of MICE on FNAC

2.11.1. Surface morphology analysis of FNAC and MICE-FNAC using Scanning electron microscopy (SEM)

The surface morphology of FNAC and MICE-FNAC was determined using Leo-Jeol Scanning Electron Microscope with magnification of 2500–10,000×. The FNAC samples were coated with gold by a gold sputtering device for the clear visibility of the surface morphology.

2.11.2. Fourier Transform- Infrared spectroscopic studies

An infrared spectrophotometer (Perkin-Elmer) was used for the investigation of the surface functional groups. The samples with KBr (spectroscopic grade) pellets were prepared with the dimensions diameter, 10–13 mm and thickness, 1mm. The free MICE, FNAC and MICE-FNAC were scanned in the spectral range of 4000–400 cm^{-1}.

2.11.3. XRD pattern analysis

The XRD pattern of free MICE, FNAC and MICE-FNAC was determined with high resolution GUINER powder X-ray diffractometer (SEIFERT, Germany).

2.11.4. Thermal characterization of MICE and MICE-FNAC

Required quantity (8-10 mg) of lyophilized MICE, FNAC or MICE-FNAC samples were loaded in platinum TGA pan and thermo gravimetric analysis was made under pure nitrogen atmosphere, from 0°C to 800°C at a temperature gradient of 10°C/min. The thermogram was routinely recorded as duplicates using TGA Universal V4.4A (TA instruments).

DSC analysis was carried out by loading the required quantity (8-10 mg) of lyophilized MICE, FNAC or MICE-FNAC samples was loaded in aluminum DSC pan and thermo gravimetric analysis was carried out under reduced nitrogen atmosphere from 0°C to 200°C at a temperature gradient of 10°C/ min. Scans were routinely recorded as duplicates using DSC Q200 (V23.10 Build 79, TA instruments).

2.12. Kinetic studies on the degradation of NPG by MICE-FNAC

The degradation study was carried out with the immobilized MICE on FNAC in a batch reactor. The degradation experiment was conducted at different variables such as the contact time (5-210 min), pH (1- 10), temperature (20^{o} to 80^{o}C), agitation speed (30-150 rpm) and initial concentration of NPG (5 – 25 µM). The effect of contact time was determined by mixing 10 µM

of NPG with 1 g of MICE-FNAC in 10 ml phosphate buffer of pH 7 and they were incubated at 35ºC under mechanical agitation of 150 rpm. The samples were withdrawn at different time intervals (5 to 210 min) and UV-Visible spectra were recorded using a UV-visible spectrophotometer (Cary varion; Agilent Technologies, Middleburg, Netherlands).

The optimum pH was determined by incubating the reaction mixture at various pH ranging from 1 to 10 at room temperature in the following buffers: 0.1M KCl/HCl buffer (pH 1.0, 2.0), 0.1M Acetate buffer (pH 3.0, 4.0 and 5.0,), 0.1 M Phosphate buffer (pH 6.0, 7.0, and 8.0), 0.1 M Tris buffer (pH 9 and 10) at optimum time, 60 min & temperature, 35ºC under mechanical agitation at 150 rpm. The optimum temperature was determined by incubating the reaction mixture at different temperatures ranging from 20 to 80°C at optimum time, 60 min; pH, 7 under mechanical agitation at150 rpm. The optimum initial concentration of NPG was determined by incubating the reaction mixture with varied concentration of NPG (5- 25 µM) with 1 g of MICE-FNAC at optimized contact time, pH and temperature. The agitation speed (30-150 rpm) was optimized for the degradation of NPG using MICE-FNAC at optimized time, pH, temperature and initial concentration of NPG.

2.13. Effect of metal ions on the degradation of NPG using MICE-FNAC

NPG (20 µM) was added to the solution of volume 15ml containing 1mM of KCl, $CaCl_2.2H_2O$, $ZnCl_2$, $MgCl_2.6H_2O$, $CuSO_4.5H_2O$, $(NH_4)_6Mo_7O_{24}\cdot 4H_2O$ & VCl_3 and incubated at 40º C for 1 h to determine the stimulatory or inhibitory effects of metal ions on degradation of NPG by MICE-FNAC. The NPG with 15 ml of 0.1 M phosphate buffer (pH 7.0) solution alone served as control.

2.14. Instrumental techniques for the NPG degradation by MICE-FNAC

The NPG upon degradation by MICE-FNAC was supported by the instrumental techniques including high-pressure liquid chromatography (HPLC) and fluorescence spectroscopy. The final end product of enzymatic breakdown of NPG was also confirmed using Fourier transform infrared spectroscopy (FTIR), nuclear magnetic resonance spectroscopy (NMR) and Gas chromatography-mass spectroscopy (GC-MS).

2.14.1. Fluorescence spectroscopy

NPG is fluorescence inactive and the fluorescence spectrum was recorded using a fluorescence spectrophotometer in the wavelength range 200-800 nm (Cary Eclipse; Agilent Technologies, Middleburg, Netherlands). The fluorescence spectrum of NPG degraded by MICE-FNAC was also recorded. The enzymatic reaction mixtures were pre-scanned using the fluorescence spectrophotometer to study the excitation and emission characteristics of both NPG and the degraded products.

2.14.2. FT-IR for spectroscopic confirmation of degradation of NPG using MICE-FNAC

The functional groups present in the initial NPG and the MICE-FNAC degraded NPG were identified using FT-IR spectrophotometer (Perkin Elmer). The samples were lyophilized and pellets were prepared with spectroscopic grade KBr of dimensions diameter, 10mm and thickness, 1 mm. The spectrum was analyzed in the spectral range of 400-4000 cm^{-1}.

2.14.3. High performance liquid chromatography (HPLC)

The degraded compounds of NPG were quantified using HPLC with a PDA detector at λ_{294} nm (Shimadzu). The sample injection volume of 100 µl was separated using cartridge containing C18 column. The mobile phase used was methanol and water in the ratio 95:5 and was applied at a flow rate of 1 mL/min.

268 **2.14.4. Nuclear Magnetic Resonance (NMR) spectroscopy**

269 The sample preparation for NMR analysis was carried out by dissolving 5 to 30 mg of
270 lyophilized samples in 650µl of Deuterated DMSO (Brucker NMR FT 500 mHz). The degraded
271 products of NPG were identified using ^{1}H and ^{13}C NMR analyses.

272 **2.14.5. GC-MS analysis**

273 GC-MS analysis of NPG and the NPG degraded by MICE-FNAC was carried out in
274 Agilent 7000 QQQ (USA). Mass spectra were analysed in the range of 60–650 atom mass units
275 (amu) at the rate of 90 scans min^{-1} for a run time of 40min.

276 **3. Results and Discussion**

277 **3.1. Isolation and identification of bacteria by phylogenetic analysis**

278 The soil site selected for isolation of bacteria was acclimatized with NPG for about 45
279 days. The acclimatized soil sample was inoculated into minimal media (M9, HiMedia)
280 containing NPG as the sole carbon source. After 3 days of incubation, the above sample was
281 used as an inoculum for the fresh medium containing NPG. The process was repeated for several
282 times in order to isolate a microorganism for degradation of NPG with high efficiency. The
283 guanine-cytosine richness in the bacterial genome, an important factor in characterizing a
284 species, was about 20-75%.[45] The isolated microorganism was found to be highly stable with
285 53.46% guanine–cytosine content. The microorganism was isolated for the production of
286 intracellular enzymes. The 16SrDNA sequencing data confirmed that the isolated organism was
287 *Serratia marcescens. S. marcescens* is a red pigmented bacterium that grows at pH, 7 and
288 temperature, 35º C.

289

290

3.2. Extraction and purification of MICE

The MICE extracted from *S. marcescens* were purified and run on SDS-PAGE to determine their molecular weight. The SDS-PAGE analysis showed that there were several bands of enzymes present with different molecular weight. The MICE was found to contain the following enzymes: Catechol dioxygenase (1.141 Umg^{-1}), Phenol hydroxylase (1.255 U mg^{-1}), Dehydrogenase (0.081 U mg^{-1}), Alkaline phosphatase (1.92 U mg^{-1}), Pyruvate decarboxylase (2.761 U mg^{-1}), Pyruvate kinase (2.296 U mg^{-1}) and Nitrate Reductase (2.15 U mg^{-1}).

3.3. Identification of MICE

The molecular weights of various enzymes present in the mixed intracellular enzymes were identified by SDS-PAGE (Fig.2). The molecular weight of extracted enzymes were as follows: 1,2- Catechol dioxygenase, 38kDa; Phenol hydroxylase, 28kDa; Dehydrogenase, 109 kDa; Alkaline phosphatase, 70kDa; Pyruvate decarboxylase, 71kDa; Pyruvate kinase, 63kDa; and Nitrate reductase, 156 kDa.

3.4. Aminoacid composition of MICE

The amino acid composition of MICE was determined using HPLC as shown in Table 1. It was found that the MICE contained polar amino acids by 60.0%, non polar amino acids by 27.4% and aromatic amino acids by 13%. The aminoacids such as aspartic acid, glutamic acid, serine and histidine are very important in functioning of the protein as they constitute the catalytic triad of the various intracellular enzymes.[46]

3.5. Immobilization of MICE on FNAC

The effect of time on the immobilization of MICE was carried out to determine the equilibrium values. The activity of MICE and protein content were measured at different time intervals (30 to 210 min) during the process of immobilization with 2 mg of lyophilized MICE at

pH 7 and at 35º C (Fig.3a). It was found that, the immobilization was rapid up to 90 min and then there was a slight increase in immobilization until the equilibrium (150 min) was attained. Initially, the number of adsorption sites available was higher and the driving force for the mass transfer of MICE was greater. As the immobilization time was increased, the number of bare active sites became less and the MICE molecules might become clustered inside the FNAC particles, thus impairing the diffusion of MICE. The initial protein content of MICE was found to be 1065.8 mg and the immobilization capacity of FNAC was 643 mg/g of the matrix.

The experiments were carried out at were carried out at a wide range of pH values between pH 1 and 10 for MICE of initial protein content of 1065.8 mg and temperature 35^{o}C in order to determine the optimum pH for the immobilization of the MICE onto FNAC. The immobilization of MICE on FNAC was found to be the maximum at pH 7 with immobilization capacity of 643mg/g as shown in Fig. 3b. Immobilization outside this pH range was decreased, may be attributed to the factors that the enzyme may become denatured or lose its tertiary structure, and, therefore, lose its ability to function as a catalyst for the enzymatic reactions.

The optimum temperature for the immobilization of MICE onto FNAC was determined by varying the temperature from 20 to 60 ºC at an initial MICE activity (1065.8 mg) at their optimum pH 7. The immobilization of MICE on FNAC was found to be the maximum at 40 ºC. At 40º C temperature, the maximum loading achieved was 705 mg/g of FNAC (Fig.3c). The reaction rate decreased beyond the optimum temperature owing to denaturation of enzymes and thereby lost its ability to function as a catalyst in the enzymatic reaction.

The immobilization capacity of FNAC was found to increase with increase in the initial MICE concentration, however, the percentage immobilization decreased with increase in MICE concentration. The optimum MICE concentration was found to be 4 mg (2131.6 mg of protein)

with the immobilization capacity of 1287mg/g of FNAC at the optimum pH and temperature (Fig. 3d). The high immobilization capacity of FNAC may be due to more number of anchoring sites in the matrix.

The optimum particle size of FNAC for the immobilization of MICE was determined by varying the particle size as 100, 3 00, 400 & 600 µm at the optimum conditions pH, 7; temperature, 40ºC and MICE concentration, 4 mg (2131.6 mg of protein). The immobilization capacity of FNAC was increased with decrease in the particle size of FNAC. The optimum particle size of FNAC was found to be 300 µm with the immobilization capacity of 1645mg/g of FNAC at the optimum conditions (Fig. 3e).

The optimum mass of FNAC for the immobilization of MICE onto FNAC was determined by varying the mass (0.5 to 2.5 g) at the optimum conditions pH, 7; temperature, 40ºC; MICE concentration, 4 mg (2131.6 mg of protein) and FNAC particle size, 300µm. The optimum mass of FNAC was found to be 1g with the immobilization capacity of 1645mg/g of FNAC at the optimum conditions (Fig. 3f).

Thus, the optimum conditions required for the maximum immobilization of MICE on FNAC was found to be time, 150 min; pH, 7; temperature, 40ºC; MICE concentration, 4 mg (2131.6 mg of protein); FNAC particle size, 300µm and mass of FNAC, 1g with the immobilized MICE capacity of 1645mg/g .

3.5.1. Adsorption Isotherms

Adsorption data are represented by isotherms and they were used in determining the immobilization of MICE on FNAC. In the present study, the Langmuir and Freundlich isotherm models were deliberated for this purpose. The Langmuir isotherms were developed based on an

assumption that monolayer adsorption onto a surface containing a finite number of adsorption sites with uniform energies of adsorption. It is represented as follows (Eq. 5)) [49].

$$q_{e=} \frac{K_L C_e}{1 + bC_e} \quad (5)$$

q_e (mg/g) and C_e (mg/L) are the amount of MICE adsorbed per unit weight of FNAC and equilibrium liquid phase concentration respectively. K_L (L/g) and b (L/mg) are the Langmuir adsorption constants (Table 2). The essential features of the Langmuir isotherm can be expressed in terms of a dimensionless constant called separation factor, R_L (also called equilibrium parameter), defined by Eq. (6).

$$R_L = \frac{1}{1 + K_L C_o} \quad (6)$$

C_o (mg/L) is the initial MICE concentration. The value of R_L indicates the shape of the isotherms to be either unfavourable ($R_L > 1$), linear ($R_L = 1$), favorable ($0 < R_L < 1$) or irreversible ($R_L = 0$).

The Freundlich isotherm can be applied to non-ideal adsorption onto heterogeneous surfaces as well as multilayer sorption and is expressed by Eq. (7).

$$q_e = K_F C^{\frac{1}{n}} \quad (7)$$

'K_F' (mg/g)(ml/mg) is the Freundlich constant related to adsorption capacity of FNAC and 'n' is the Freundlich exponent (Table 2).

The adsorption isotherms indicated that immobilization of MICE on FNAC obeyed Freundlich isotherm model based on the regression coefficient (R^2). The value of R_L, the separation factor fell in the range of less than zero, indicating that the immobilization of MICE on FNAC was irreversible. This confirmed the immobilization of MICE, through the formation of a strong bonding with adsorption sites of FNAC.

3.5.2. Nonlinear kinetic model for the immobilization of MICE on FNAC

The validity of kinetic order for the immobilization of MICE on FNAC process was based on the regression coefficients and χ^2 values. The experimental data were plotted under each model (Figures not shown). The values of k_1, k_2 and q_e for each sorption process were determined from the slopes and intercepts of the plots and they are presented in Table 3 along with their relevant regression coefficients (R^2). Relatively higher R^2 values, least χ^2 values and more or less closer experimental q_e and calculated q_e values showed a better agreement of immobilization of MICE on FNAC with the pseudo second order kinetic model (Fig.4). The pseudo second order kinetic model suggests that the rate of this adsorption process depend both on concentration of MICE and adsorption sites of FNAC.

3.6. Thermodynamic studies for immobilization of MICE on FNAC

The thermodynamic parameters were calculated using the Eq. (4). The change in positive entropy value (ΔS° = 0.256 kJ/molK) indicates that the immobilization of MICE on FNAC was accompanied with increased random distribution of it at standard temperature, 25ºC. Moreover, the negative value of enthalpy (ΔH° = -78.19 kJ/mol) of the system indicates the immobilization of MICE on FNAC was an exothermic process at 25ºC. The negative free energy (ΔG° = -153.20 kJ/mol) value indicates the immobilization of MICE on FNAC was spontaneous at 25ºC.

3.7. Evidences for the immobilization of MICE on FNAC

3.7.1. SEM morphology of FNAC and MICE-FNAC

The SEM images of FNAC (Fig.5a) reveal that the surface was covered with an epitaxially grown deposit on the outer pore surface area and the chemical deposit was uniform in nature with regard to the opacity. This may be regarded as an amino– aldehyde chemical deposit

on the nanoporous activated carbon surface. The surface morphology of MICE-FNAC shows that the MICE have been immobilized onto the walls of the pores of FNAC (Fig.5b).

3.7.2. Fourier Transform- Infrared spectroscopic studies

The FT-IR spectrum of purified MICE is shown in Fig.6a. The FT-IR spectrum of MICE shows major protein bands (due to vibration of the peptide linkage) in the spectral region of 1200–1700 cm^{-1}. The band at 1635.49 cm^{-1} is due to the C=O stretching vibrations of amide I. The bands at 3434 cm^{-1} and 1547.03 cm^{-1} may be attributed to N-H stretching and C–N bending. The bands at 633.59 cm^{-1} and 662.85 cm^{-1} may be attributed to C-N stretching vibrations in MICE. The bands at 2925.88 cm^{-1} and 2855.09 cm^{-1} may be due to the asymmetrical and symmetrical C-H stretching of methylene groups respectively. The band at 1162.55 cm^{-1} may be attributed to C-O stretching vibrations present in MICE

The FT-IR spectrum of FNAC shows the peak corresponding to the N–H stretching vibration of a secondary amine at 3416.26 cm^{-1}. The significant increase in the intensity of the band at 1715.57 cm^{-1} in FNAC corresponds to C–O stretching vibrations of carbonyl or aldehyde groups. The bands at 2923.82 cm^{-1} and 1365.59 cm^{-1} may be attributed to methylene stretching and bending vibrations respectively. This may be due to the addition of ethylenediamine and glutaraldehyde during the preparation of FNAC. This confirms the condensation of ethylenediamine and glutaraldehyde onto Nanoporous activated carbon.[42]

The FT-IR spectrum of MICE-FNAC (Fig. 6c) showed that the frequency at 1652.34 cm^{-1} may be attributed to amide I of immobilized MICE. The peak corresponding to C-O stretching vibration (1715.57 cm^{-1}) in MICE-FNAC of ketone and aldehyde groups were masked because of the strong binding of NH_2 group of the MICE with the aldehyde group of FNAC. The

wide peak observed at 3414.43 cm^{-1} in MICE-FNAC is due to the N-H stretching vibration of secondary amine.

3.7.3. XRD pattern of MICE, FNAC and MICE-FNAC

The XRD patterns of the MICE, FNAC and MICE-FNAC are shown in Fig. 7 a, b and c respectively. The XRD pattern of MICE (Fig. 7a) suggests its crystalline nature with diffracting peaks of 2θ angle at 10.88, 16.67, 17.36, 23.76, 26.55, 28.21, 31.13, 33.08, 35.30, 36.14, 39.61, 43.23, 51.02, 53.80, 63.26 and 66.04° due to presence of the mixed enzymes. The XRD pattern of FNAC (Fig. 7b) contains peaks corresponding to 2θ values at 11.3, 12.9, 15.8, 18.0, 20.1, 22, 25.05, 25.6, 26.6 and 30.9° due to surface functionalization (Ramani et al., 2012). The immobilization of MICE in FNAC (Fig. 7c) was further confirmed with XRD pattern, which showed the peaks at 12.9°, 19.46 and 22° due to surface functionalization and peaks at 2θ values of 10.69, 14.11, 21.26, 23.62, 27.37, 48.52, 52.58 and 62.98°confirmed the presence of MICE in MICE-FNAC.

3.7.4. Thermogravimetric analysis of MICE, FNAC, MICE-FNAC

The thermogram of MICE (Fig. 8a) showed 8.91% weight loss at 114.45°C due to the removal of moisture. A major weight loss occurred from 196.32 to 563.06°C due to the decomposition of the major components of the MICE. At the end of the scan (800°C), 39.62% of the sample remained as fixed residue indicating the thermal sensitivity of the constituents of MICE.

The TGA of FNAC (Fig.8b) showed 3.17% weight loss at 101.34°C due to the removal of moisture. A major weight loss occurred from 194.24 to 533.58°C and 62.05% of the sample remained as fixed residue at 800°C, indicating the thermal resistance of the constituents of FNAC.

The thermogram of MICE-FNAC (Fig. 8c) showed 8.05% weight loss at 90.31°C due to the removal of moisture. A weight loss of 9.64 % was observed at 190.39°C which could be due to decomposition of smaller particles in MICE. A major weight loss occurred from 215.12°C to 376.89°C is due to the decomposition of the major components of the MICE-FNAC. At the end of the scan (800°C), 62.60% of the sample remained as fixed residue, indicating the higher thermal resistance of the constituents of MICE-FNAC than MICE.

The DSC of MICE (Fig. 8d) shows that there was an endothermic transition at 75.97°C, 208.05°C with the enthalpy of transition 144.7 J/g and 187.2 J/g respectively. The DSC of FNAC (Fig.8e) shows there was a thermal transition at 118.09°C with the enthalpy of transition 203.9 J/g. The DSC of MICE-FNAC (Fig. 8f) showed a sharp endothermic thermal transition at 111.38°C and small bumps at 171.34°C & 233.33°C with the enthalpy of transition 178.9 J/g.

These results suggest that the the thermal stability of the MICE was enhanced due to the stabilized bonding between MICE and functional groups of FNAC. And also the results suggested that there was not much change in their enthalpy of transition, indicating that the nature of MICE was not being altered upon immobilization.

3.8. Degradation kinetics of NPG using MICE-FNAC

The effect of various factors such as contact time (5-210 min), pH (1- 10), temperature (20^{o} to 80^{o}C), agitation speed (30-150 rpm), initial concentration of NPG (5- 25 µM) was studied on degradation of NPG using 1 g of immobilized MICE (1645mg/g of FNAC). The degradation of NPG as a function of time (Fig.9a) shows the disappearance of characteristic peak of NPG (λ_{390} nm) with increase in time and increase in the intensity of the formation of new compound at λ_{290} nm using MICE-FNAC. The degradation of NPG using free MICE also showed the disappearance of characteristic peak of NPG (λ_{390} nm) and the formation of new compound at

λ_{290} nm (Fig.9a). The maximum degradation was attained in 3 h at pH, 7; temperature, 30ºC; initial NPG concentration, 10 µM with agitation speed of 70 rpm. The degradation of NPG using FNAC was used as the control; where there is no formation of new compound at λ_{290} nm suggesting MICE mediates the degradation of NPG.

The effect of pH on the degradation of NPG using MICE-FNAC was studied. It was observed that MICE- FNAC was able to degrade NPG at different pH conditions from 1-10 (Fig.9b) and the maximum degradation of NPG was observed at pH 7.0 using MICE- FNAC. This also suggests that the carrier matrix, FNAC provides MICE the ability to retain the geometry from denaturation despite the wide fluctuations in pH. The chemical resistance of MICE in its immobilized state may be correlated with the strong binding established with FNAC.

The effect of temperature on the degradation of NPG using MICE-FNAC was studied. The NPG degradation increases with increase in temperature. It was observed that the MICE-FNAC could withstand wide range of temperatures. The intensity of formation of new compound varied but the degradation of NPG was achieved. It was observed that the characteristic peak of NPG at λ_{390} nm was reduced in its intensity and a new peak appeared at λ_{290} nm indicating partial degradation of NPG at 20ºC (Fig.9c). The peak at λ_{390} nm was completely disappeared at 30 ºC and the maximum amount of new compound at λ_{290} nm was found at 40ºC. As the temperature increased, the intensity of characteristic peak at λ_{390} nm decreased progressively and the intensity of new peak at λ_{290} nm increased steadily.

The initial concentration of NPG (Fig.9d) was varied and it was found that the optimum concentration of NPG was about 20 µM to obtain the maximum concentration of new compound. The effect of agitation speed on degradation of NPG using MICE-FNAC was studied. It was observed that there was a small peak at λ_{390} nm and a new peak at λ_{290} nm indicating partial

degradation of NPG at agitation speed of 30 rpm (Fig.9d). As the agitation speed increased, the peak at λ_{390} nm was completely eliminated but a new compound of high intensity appeared at 70 rpm.

The optimum conditions for the degradation of NPG using MICE-FNAC was found to be time, 3h; pH, 7; temperature, 40ºC, initial concentration of NPG, 20 µM and agitation speed, 70 rpm.

3.9. Effect of metal ions

Most enzymes require the presence of metal ion activators to express their catalytic activity. Metal ions act as cofactors for many enzymes to increase their catalytic activity at lower concentrations while the catalytic activity was reduced due to the toxic effect of metal ions at high concentrations.[47] The effect of various metal ions such as K^+, Zn^{2+}, Cu^{2+}, Ca^{2+}, Mg^{2+}, Mo^{6+} and V^{3+} on the degradation of NPG using MICE-FNAC was studied in the present investigation. Zn^{2+}, Cu^{2+}, Ca^{2+} and V^{3+} enhanced the catalytic effect on degradation of NPG using MICE-FNAC (Fig.10). All other metal ions inhibited the degradation of NPG as evidenced from the absence of new compound formation at λ_{290} nm. The metal ions such as Zn^{2+}, Cu^{2+}, Ca^{2+} and V^{3+} had stimulatory effect on the degradation of NPG were used in combination (Fig.10). The intensity of new compound formed at λ_{290} nm was in the decreasing order as V^{3+} > all metal ions> Cu^{2+}> Ca^{2+}> Zn^{2+} ions.

The MICE from *S.marcescens* such as dehydrogenase and alkaline phosphatase could be enhanced by the presence of zinc ion.[46] Copper ion enhanced the activity of dioxygenase,[48] while the kinase was activated by calcium and reductase by vanadium ion.[49] In protein metal-binding sites, the metal ion is coordinated by different combinations of protein side chains, including the

nitrogen of histidine, the oxygen of aspartate or glutamate and the sulfur of cysteine; among these, histidine is the most commonly observed, followed by cysteine.[50]

The Zn^{2+} activates alkaline phosphatase by binding to the ligands three histidine and two water molecules, while Zn^{2+} activates dehydrogenase enzyme by binding with two cysteine, one histidine and a water molecule. Copper ion activates dioxygenase by forming square planar coordination with two histidine, one cysteine and a water molecule while calcium ion forms a octahedral coordination with two aspartate residues (or one aspartate and one asparagine) bound in a monodentate manner, one glutamate residue bound in a bidentate manner, one main-chain carbonyl group and one water molecule. The sixth ligand is variable and may be water, serine, asparagine or aspartate.[51] Vanadium ion activates reducatase by binding with the carboxylate groups in asparate, glutamate and cysteine molecules. The metal ion in the active site of intracellular enzymes causes polarisation of hydrogen–oxygen bond, making the oxygen slightly more negative, thereby weakening the peptide enhancing the enzyme activity.[52]

3.10. Instrumentation evidences for the degradation of NPG

NPG was treated with MICE- FNAC at the optimized conditions and the degradation was studied using the following instrumentation techniques.

3.10.1. Flourescence spectroscopy

The fluorescence spectra of NPG and degraded NPG using MICE-FNAC in the presence of Zn^{2+}, Cu^{2+}, V^{3+}, Ca^{2+} ions and all metal (AM) ions are shown in Fig.11. NPG is a fluorescent inactive compound as shown in Fig. 11a. The fluorescence spectra of NPG degraded by MICE-FNAC in the presence of Zn^{2+},Cu^{2+}, V^{3+} and Ca^{2+} ions showed that fluorescent active compounds were formed with excitation and emission peaks around λ_{340} nm and λ_{410} nm respectively (Fig.11). The presence of an emission peak in the spectrum could be due to the

538 complete destruction of NPG and the formation of fluorescence active end products. Thus, the
539 fluorescence spectra confirm the degradation of NPG by MICE- FNAC in the presence of Zn^{2+},
540 Cu^{2+}, V^{3+}, Ca^{2+} ions and AM ions.

541 **3.10.2. FT-IR spectra of NPG and degraded NPG by MICE- FNAC**

542 The FT-IR spectrum of NPG (Fig.12a) shows the characteristic peaks. The bands at
543 1489.48 cm^{-1} and 1646.17 cm^{-1} are attributed to stretching vibrations of C=C in aromatic ring.
544 The bands at 1549.43 cm^{-1} and 1588.17 cm^{-1} are due to the asymmetric stretching vibrations of
545 N=O in nitro group. The band at 1312.91cm^{-1} is attributed to symmetric N=O stretching vibration
546 in nitro group. The stretching of aromatic C-H is observed at 3096.1 cm^{-1}. The C-N stretching in
547 NPG is confirmed at 836.67 cm^{-1} and 699.02 cm^{-1}. The bands at 770.25 cm^{-1}, 520.92 cm^{-1},
548 470.13 cm^{-1} are due to the out of plane bending vibrations of C-H in aromatic ring. The inplane
549 aromatic C-H bending vibrations were confirmed at 1081.8 cm^{-1} and 1015.6 cm^{-1}. The band at
550 3456.25 cm^{-1} is attributed to the strong bonded O-H vibrations.

551 The degradation of NPG by MICE-FNAC was confirmed from the FT-IR spectrum
552 (Fig.12b). The band at 1642.17 cm^{-1} is attributed to asymmetric stretching of carboxylate ion in
553 degraded sample. The peak at 1450.3 cm^{-1} is attributed to asymmetric bending of CH_3 group.
554 The band at 3436.68 cm^{-1} is due to the stretching of O-H group. The peak at 1084.12 cm^{-1} may
555 be attributed to stretching of C-O group. The FT-IR spectrum confirmed the degradation of NPG
556 and the presence of a keto group concludes the degraded end product could be pyruvic acid.

557 **3.10.3. High-performance liquid chromatography**

558 The HPLC chromatogram of NPG and NPG after degradation is shown in Fig.13. The
559 HPLC chromatogram of the initial NPG shows a compound with retention time (Rt) at 9.6 min.
560 Figure (13b) shows that the retention time of the parent compound disappeared and new peaks

were appeared at retention time (Rt) of 8.6, 8.3 & 1.2 min. This confirms the degradation of NPG by MICE- FNAC, which is further confirmed with H^1 and ^{13}C NMR spectroscopy.

3.10.4. ^1H &^{13}C Nuclear Magnetic Resonance spectroscopy

The ^1H NMR spectrum of NPG was scanned between δ 0 and δ 12 ppm. The ^1H-NMR spectrum showed signals in the aromatic region around δ 6.4 and 6.6 ppm which indicates hydrogen attached to substituted benzene skeleton. The chemical shift around δ 4.0 ppm can be assigned to the proton in OH group attached to aromatic ring (Fig. 14a). The MICE-FNAC degraded NPG shows the presence of aliphatic proton at δ 3.4 and δ 3.8 ppm.

The ^{13}C NMR spectrum of NPG was scanned between δ 0.0 and δ 200 ppm. The chemical shift around δ 130–140 ppm indicates the evidence for phenyl carbon in the aromatic ring (Fig. 15a). The occurrence of chemical shifts at δ 118.45, δ 118.22 and δ 115.41 ppm confirm the presence of carbon atoms attached to hydroxyl groups. The chemical shift at δ 78.93 ppm can be assigned to the carbon attached to nitro groups. The ^{13}C-NMR spectrum of MICE-FNAC degraded NPG sample shows that the peaks around δ 110-140 ppm were disappeared. The chemical shift at δ 208 ppm indicates the evidence for keto carbon. The chemical shift at δ 18.71 ppm indicates the evidence for methyl carbon (Fig. 15b). The absence of carboxylic peak δ 180 ppm may be due to the masking effect of the solvent. The absence of peaks at δ 78.93, 118.45, δ 118.22 and δ 115.41 ppm confirms the degradation of NPG by MICE-FNAC.

3.10.5. GC-MS spectra of NPG before and after degradation by MICE-FNAC

GC-MS analysis was used to identify the end products of NPG degraded by MICE-FNAC. The molecular ion [M+] at m/z=173.9 with a retention time of 10.93 min was found to be identical to the mass spectral properties of the standard NPG (Fig. 16a). The mass spectrum data of NPG shows the fragment peak of $C_6H_5O_4$ (i.e. 141) on elimination of neutral NO molecule

584 with a rearrangement to form the phenoxy cation (m/z =143.1). The MS data show the molecular
585 ion at m/z= 101 could be due to the elimination of two alcohol groups.

586 The MICE-FNAC degraded NPG sample showed the presence of pyruvic acid,
587 corresponding to a molecular ion peak at m/z=88 with the retention time of 8.258 min. Pyruvic
588 acid, on fragmentation of the COOH group, yielded CH_3CO^+, corresponding to a peak at m/z=43
589 and on elimination of the CH_3 group, a peak corresponding to m/z=33 (Fig. 16b). The fragments
590 with molecular ions confirm the presence of pyruvic acid as the product of degradation of NPG
591 by MICE-FNAC.

592 The plausible pathway for the degradation of NPG by MICE-FNAC involves the
593 reduction of the nitro group in NPG by reductase to form 2-amino phloroglucinol which is
594 further converted into 2- hydroxy phloroglucinol by the elimination of ammonia catalysed by
595 monooxygenase. The next step is ring cleavage by dioxygenase to form 3, 5, dihydro muconate.
596 This intermediate was further catalysed by kinase, dehydrogenase, phosphatase and pyruvate
597 decarboxylase to form non-toxic, pyruvic acid. The pyruvic acid was confirmed by functional
598 groups present in the NPG degraded sample through FT-IR spectroscopy and mass fragmentation
599 evidence from GC-MS spectroscopy.

600 **4. Conclusions**

601 The MICE from *S.marcescens,* capable of degrading NPG were extracted and
602 characterized. The mixture of intracellular enzyme was purified and the molecular weight of
603 enzymes was determined using SDS-PAGE. The optimum conditions for the immobilization of
604 MICE on FNAC was found to be time, 2.5h; pH,7.0; temperature, 40ºC; concentration of MICE,
605 4mg; particle size of FNAC, 300µm and mass of FNAC, 1 g. The SEM images showed that the
606 MICE was immobilized onto the carrier matrices. The immobilization of MICE was confirmed

using FT-IR spectroscopy and XRD pattern analysis. The thermal behaviour of the free and the immobilized MICE was studied using thermogravimetric analysis. The immobilization of MICE on FNAC followed pseudo second order kinetic model and adsorption process obeyed Freundlich model. The degradation of NPG by MICE-FNAC was optimum at contact time, 3h; pH, 7.0; temperature, 40ºC; concentration of NPG, 20 µM and agitation speed, 70 rpm. The degradation efficiency of NPG was enhanced with higher rate of conversion into pyruvic acid in the presence of metal ions (Zn^{2+}, Cu^{2+}, Ca^{2+}, V^{3+} and AM). The confirmation of the NPG degradation by MICE-FNAC was justified using UV-Visible, fluorescence, FTIR spectroscopy, HPLC, NMR and GC-MS spectroscopy.

Acknowledgments

P. Saranya is grateful to the Council of Scientific and Industrial Research (CSIR), India. The financial assistance under the STRAIT (CSC0201) programme is also gratefully acknowledged.

References

1 A.M. Soto, H. Justicia, J.W. Wray and C.P. Sonnenschein, Environ Health Persp, 1991, **92**, 167-173.

2 T.J. Kubiak, H.J. Harris, L.M. Smith, T.R. Schwartz, D.L. Stalling, J.A. Trick, L. Sileo, D.E. Doucherty and T.C. Erdman, Arch Environ Contam Toxicol, 1989, **18**, 706–727.

3 H. Rathsburg and B. Pat, Angew Chem, 1928, **41**, 1285.

4 W. Fredrich, Z. Ges and U. Schiess, Spengstoffw, 1933, **80**, 113.

5 PCT Int. Appl., WO 2002051821 A1 20020704, 2002.

6 K. Ju and R. E. Parales, Microbiol mol biol rev, 2010, **74**, 250–272.

7 S.K. Liehr, A.R. Rubin and B. Tonning, Water Environ Res, 2003, **76,** 1191–1237.

8 T. Robinson, G. McMullan, R. Marchant and P. Nigam, Bioresour Technol, 2001, **77**, 247–255.

9 P.C. Vandevivere, R. Bianchi and W. Verstraete, J Chem Technol Biotechnol, 1988, **72**, 289.

10 J.C. Sin, S.M. Lam, A.R. Mohamed and K.T. Lee, Int J Photoenergy, 2012, **23,** Doi:10.1155/2012/185159.

11 S. Sharma, J.P. Ruparelia and M. L.Patel, International Conference on Current Trends in Technology, Ahmedabad, 2011.

12 G. Tchobanoglous, F. Burton and H. Stensel, Wastewater Engineering: Treatment and Reuse, 4th Ed., 2003, New York, NY: McGraw Hill.

13 T. Oppenländer, Photochemical purification of water and air, Advanced Oxidation Processes (AOPs): Principles, reaction mechanisms, reactor concepts, 2003, Winheim, Germany: Wiley-VCH.

14 S. Kommineni, J. Zoeckler, A. Stocking, S. Liang, A. Flores and M. Kavanaugh, Advanced oxidation processes. In: National water Research Institute. URL, 2008.

15 C. S. Karigar and S. S. Rao, Decontamination, 2011, Wiley-VCH: Weinhein, pp. 1-11.

16 V. de Lorenz, R. Silva rocha, G. Carborosa, T. C. Galvao and I. Case. Sensing xenobiotic compounds: Lessons from bacteria that face pollutant in environment, 2010, pp: 81-92.

17 M. Alexander, Biodegradation and Bioremediation. 2nd Ed., 1999, Academic Press: San Diego, USA, pp. 325-327.

18 W. Fritsche and M. Hofrichter, Aerobic degradation by microorganisms, In J. Klein (ed.), Environmental processes II—soil decontamination, vol. 11b. Biotechnology, 2nd ed., 2000, Wiley-VCH, Weinheim, Germany pp. 146-155.

19 S.K. Brar, M. Verma, R.Y. Surampalli, K. Misra, R.D. Tyagi, N. Meunier and J.F. Blais, Pract Periodical Hazard Toxic Radioact Waste Management, 2006, **10**, 59-72.

20 D.V.V. Gnanasalomi, G. R. Jebapriya, J. J. Gnanadoss, Int J Comput Algorithm, 2013, **2**, 273-278.

21 S. Ecker, T. Widmann, H. Lenke, O. Dickel, P. Fischer, C. Bruhn, H.J. Knackmuss, Arch Microbiol, 1992, **158**, 149-154.

22 P. Sander, R.M. Wittalch, P. Fortnagcl, H. Wilkes and W. Francke, Appl Environ Microbiol, 1991, **57**, 1430-1440.

23 C. Nelson and M. Cox, Principles of Biochemistry, 4th Ed., 2004, W. H. Freeman, New York, pp. 47-50.

24 R. Fernandez-Lafuente, J.M. Guisan, S. Ali and D. Cowan, Enzyme Microb Tech, 2000, **26**, 568-573.

25 P.V. Iyer and L. Ananthanarayan, Process Biochem, 2008, **43**, 1019-1032.

26 J. Karam and J.A. Nicell, J chem Technol Biotechnol, 1997, **69**, 141-153.

27 M.B. Pescod, FAO Irrigation and Drainage, Food and Agriculture Organization of United nations, Rome, Italy, 1992.

28 C. Mateo, J.M. Palomo, G. Fernandez-Lorente, J.M. Guisan, and R. Fernandez- Lafuente, Enzyme Microb Tech, 2007, **40**, 1451-1463.

29 E. Kalogeris, Y. Sanakis, D. Mamma, P. Christakopoulos, D. Kekos and H. Stamatis, Enzyme Microb Tech, 2006, **39**, 1113-1121.

30 J.A. Marmur, J Mol Biol, 1961, **3,** 208-218.

31 J. Felsentein and Phylip, Bacteriology, 1993, **98,** 756-766.

32 H.N. Naiem and S.G. Jai, Res J Environ Earth Sci, 2011**, 3**, 608-613.

33 G. Cenci and G. Caldini, Appl Microbiol Biotechnol, 1997, **47**, 306–308.

34 K.M. Mayer and F.H. Arnold, J Biomol screen, 2002, **7**, 135-140.

35 H.Y. Neujahr and A. Gaal, Eur J Biochem, 1973, **35,** 386-390.

36 K.N. Fernley, The Enzymes Boger, P.D Ed., vol. 4, 1971, Academic press, New York, pp 417-447.

37 M.T. Flikweertt, L. Van Der Zanden, W.M. Janssen, H.Y. Steensma, J.P. Van Dijken and J.T. Pronk, Yeast, 1996, **12,** 247-257.

38 H. Ridley, C. A. Watts, D.J. Richardson and C.S. Butler, Appl environ microbiol, 2006, **72**, 5173–5180.

39 K. Abbe and T. yamada, J bacterial, 1982, **149**, 299-305.

40 O. H. Lowry, N. J. Rosebrough, A. L. Farr and J. Randal, J. Biol. Chem., 1951, **193**, 265–275.

41 U. K. Laemmli, Nature, 1970, **227**, 680–685.

42 K. Ramani, S. Karthikeyan, R. Boopathy, L. John Kennedy, A.B. Mandal and Sekaran G, Process Biochem, 2012, **47**, 435–445.

43 S. Lagergren and B. K. Svenska, Veternskapsakad Handlingar, 1898, **24**, 1–39.

44 Y. S. Ho and G. Mckay, Transl Chem E, 1998, **76(B)**, 183–191.

45 F. Hildebrand, A. Meyer and A. Eyre-Walker, PLos Gene, 2010, **6,** 1-9.

46 B.L. Vallee and D.S. Auld, Biochemistry, 1990, **87**, 220–224.

47 H. Rodriguez, B. de las Rivas, C. Gomez-Cordoves and R.Munoz, Int J food microbial, 2008, **121**, 92-98.

48 F. Fusetti, K.H. Schröter, R.A. Steiner, P.I. van Noort, T. Pijning, H.J. Rozeboom, K.H. Kalk, M.R. Egmond and B.W. Dijkstra, Structure, 2002, **10**, 259 – 268.

49 M. Zizic, M. Zivic, I. Spasojevic, J.B. Pristov, M. Stanic, T. Cvetic-Antic and J. Zakrzewska, Res Microbiol, 2013, **164**, 61-69.

50 D.S. Gregory, A.C.R. Martin, J.C. Cheetham and A.R. Rees, Prot Eng, 1993, **6**, 29–35.

51 J.P. Glusker, A.K.Katz and C.W. Bock,The Rigaku journal, 2000, **17**,8-16.

52 P.Saranya, R.Muneeswari and G.Sekaran, J Chem Technol biotechnol, 2014, DOI: 10.1002/jctb.4558.

Figure legends

Fig.1 Rooted phylogenetic tree showing the relationship of marine isolate *S.marcescens* to other *Serratia* sp. (values shown in the parenthesis are accession number).

Fig.2 SDS-PAGE of purified MICE from *S.marcescens* **Lane 1** Molecular weight of marker, **lane 2** Purified MICE.

Fig.3 Effect of (a) time, (b) pH, (c) temperature, (d) initial concentration of MICE, (e) Particle size of FNAC and (f) mass of FNAC on the immobilization of MICE on FNAC

Fig.4 Kinetic modelling for the immobilization of MICE on FNAC

Fig.5 SEM images of (a) FNAC and (b) FNAC-MICE

Fig.6 FT-IR spectra of (a) MICE, (b) FNAC and (c) MICE-FNAC

Fig.7 XRD pattern of (a) MICE, (b) FNAC and (c) MICE-FNAC

Fig.8 TGA of (a) MICE, (b) FNAC and (c) MICE-FNAC and DSC of (d) MICE, (e) FNAC and (f) MICE-FNAC

Fig.9 Degradation of NPG using MICE-FNAC (a) Effect of time (Experimental conditions: pH, 7; temperature, 30ºC; initial NPG concentration, 10 µM; agitation speed, 70 rpm), (b) Effect of pH (Experimental conditions: time, 3h; temperature, 30ºC; initial NPG concentration, 10 µM; agitation speed, 70 rpm), (c) Effect of temperature (Experimental conditions: time, 3h; pH, 7; initial NPG concentration, 10 µM; agitation speed, 70 rpm), (d) Effect of initial concentration of NPG (Experimental conditions: time, 3h; pH, 7; temperature, 40ºC; agitation speed, 70 rpm) and (e) Effect of agitation speed (Experimental conditions: time, 3h; pH, 7; temperature, 40ºC; initial NPG concentration, 20 µM)

Fig.10UV-Visible spectra of degradation of NPG by MICE-FNAC in the presence of metal ion enhancers

746 **Fig.11** Fluorescence spectra of (a) NPG, (b) NPG degradation using MICE-FNAC in presence of
747 vanadium (c) all metal ions (d) calcium, (e) copper and (f) zinc ions
748 **Fig.12** FT-IR spectra of (a) NPG and (b) NPG after treatment with MICE-FNAC
749 **Fig.13** HPLC chromatogram of (a) NPG and (b) NPG after degradation by MICE-FNAC
750 **Fig.14** ^{1}H NMR spectra of (a) NPG and (b) NPG after degradation by MICE-FNAC
751 **Fig.15** ^{13}C NMR spectra of (a) NPG and (b) NPG after degradation by MICE-FNAC
752 **Fig.16** GC-MS spectra of (a) NPG and (b) NPG after degradation by MICE-FNAC
753 **Fig.17** Plausible mechanism of NPG degradation by MICE-FNAC
754
755
756
757
758
759
760
761
762
763
764
765
766
767
768
769

770

771

772

773

774 **Table 1** Aminoacid composition of MICE from *S.marcescens*

Amino acids	Level (nmoles/ml)
Aspartic acid	11
Glutamic acid	91
Serine	18
Histidine	85
Glycine	248
Threonine	80
Arginine	26
Alanine	235
Tyrosine	18
Methionine	74
Valine	79
Phenylalanine	25
Isoleucine	135
Leucine	29
Lysine	150
Cysteine	97

775

776

Table 2 Isotherm parameters for the immobilization of MICE on FNAC

Langmuir constants		Freundlich constants	
K_L (L g^{-1})	3.294	K_F (mg g^{-1})(L mg^{-1})	0.513
b (L mg^{-1})	5.868	n	3.12
R^2	0.8627	R^2	0.9349
R_L	$2.8*10^{-4}$		

Table 3 Comparison of pseudo first- and second-order kinetic parameters of immobilization of MICE on FNAC (initial MICE activity, 1065.8 mg; pH, 7.0; temperature, 40ºC; particle size, 300µm; mass of FNAC, 1g and agitation, 150 rpm)

Temperature (ºC)	q_e (exp) (mg/g)	Pseudo first order				Pseudo second order			
		k_1(min^{-1})	q_e (Cal) (mg/g)	R^2	χ^2	k_2 (mg^{-1} g min^{-1})	q_e (Cal) (mg/g)	R^2	χ^2
20	223	0.0057	248	0.973	2.63	$3.17*10^{-5}$	230	0.996	0.21
30	456	0.0194	467	0.943	0.26	$2.42*10^{-5}$	450	0.969	0.08
35	643	0.0201	701	0.970	4.80	$1.26*10^{-5}$	652	0.998	0.12
40	705	0.0203	789	0.980	8.94	$1.20*10^{-5}$	692	0.999	0.24
50	546	0.0117	623	0.487	9.52	$1.06*10^{-5}$	554	0.942	0.12
60	210	0.0124	305	0.852	29.5	$2.46*10^{-5}$	254	0.983	7.62

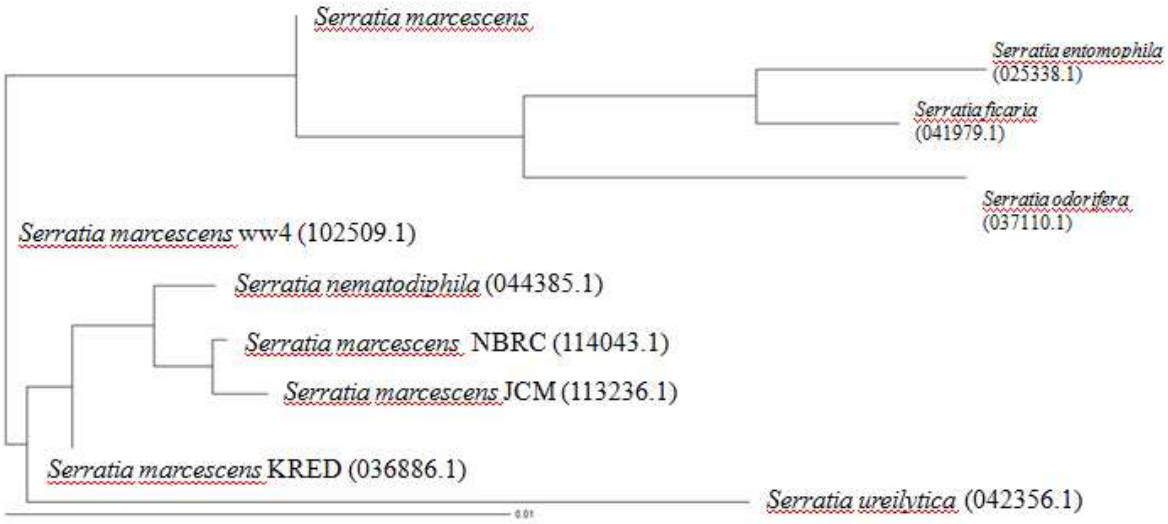

Fig.1 Rooted phylogenetic tree showing the relationship of marine isolate *S.marcescens* to other *Serratia* sp.

(values shown in the parenthesis are accession number)

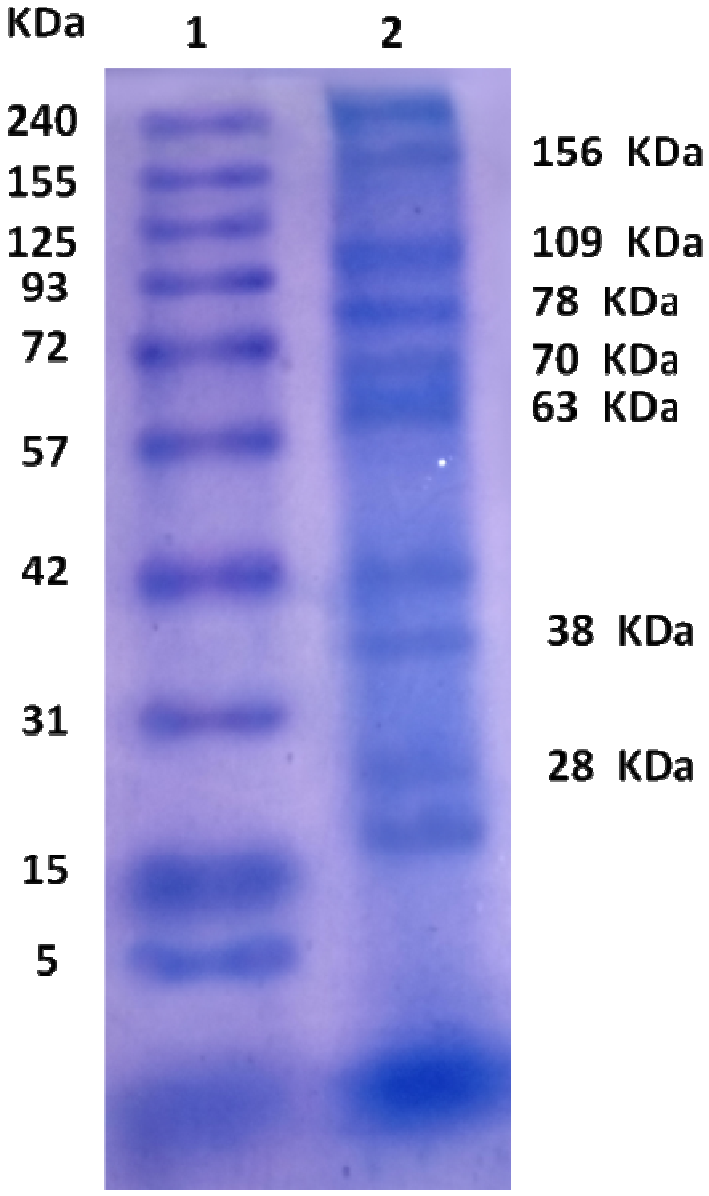

Fig.2 SDS-PAGE of purified MICE from *S.marcescens* **Lane 1** Molecular weight of marker, **lane 2** Purified MICE.

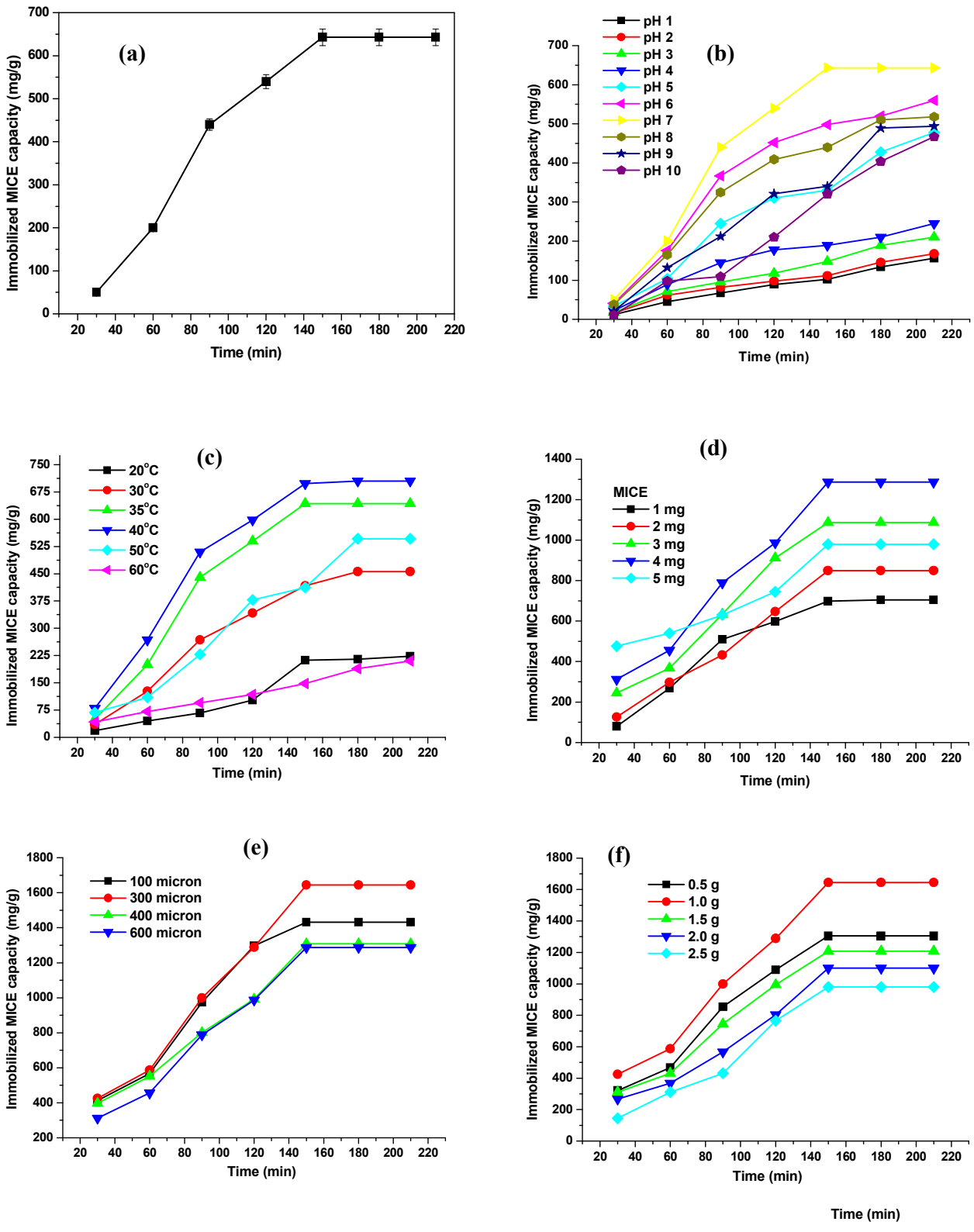

Fig.3 Effect of (a) time, (b) pH, (c) temperature, (d) initial concentration of MICE, (e) Particle size of FNAC and (f) mass of FNAC on immobilization of MICE in FNAC

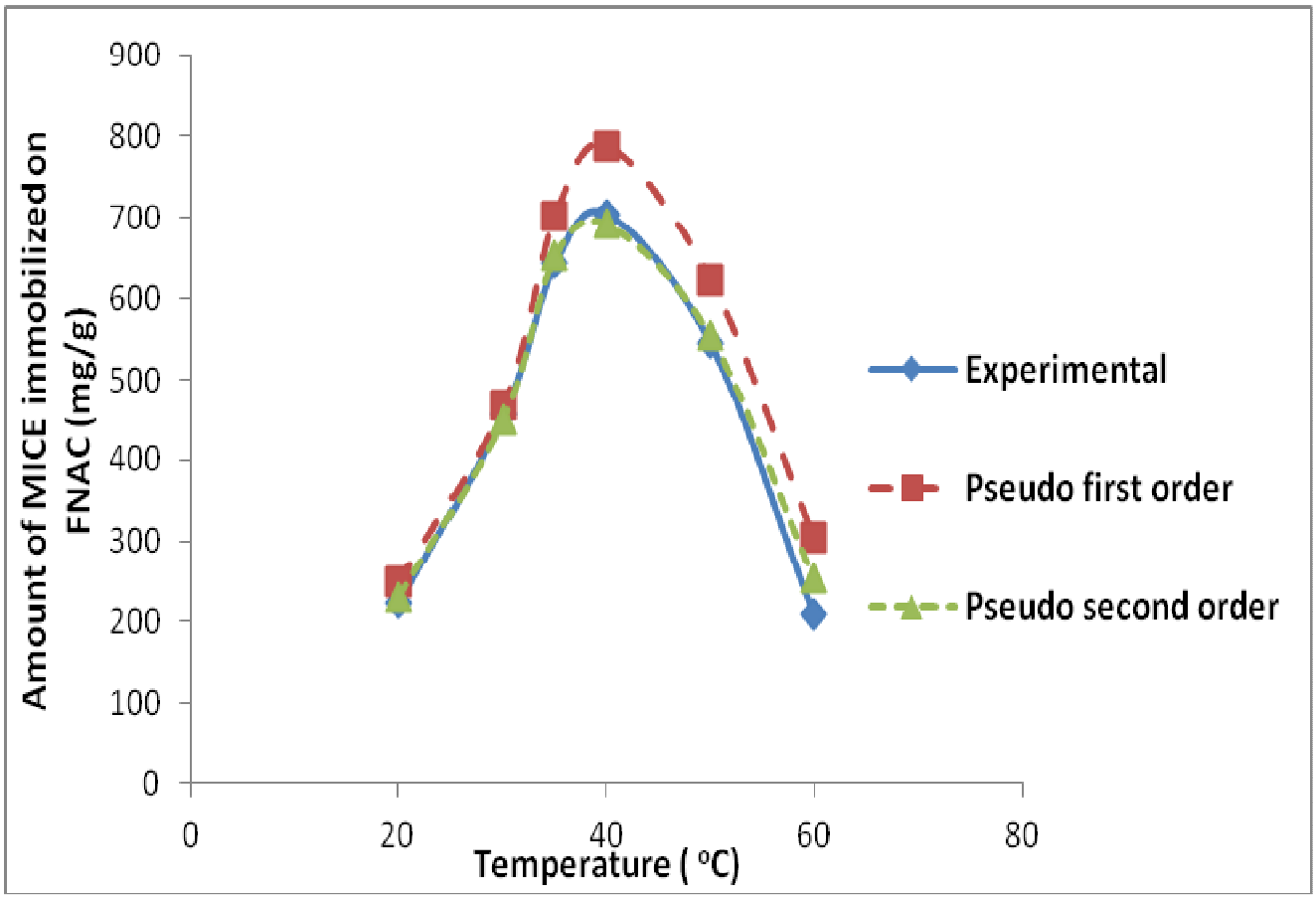

Fig.4 Kinetic modelling for the immobilization of MICE on FNAC

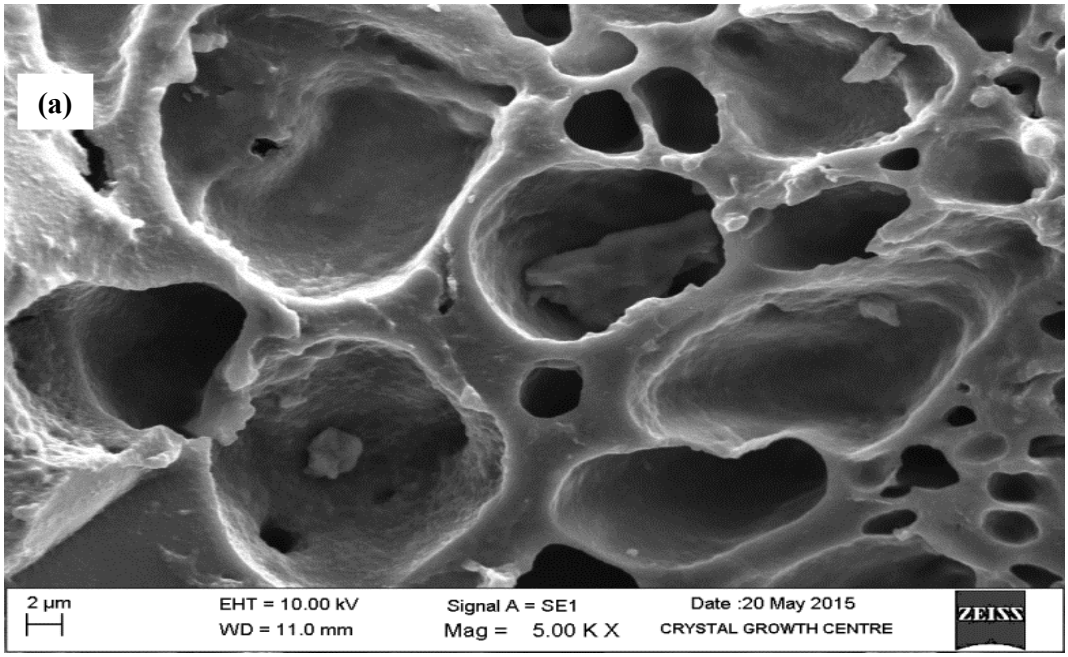

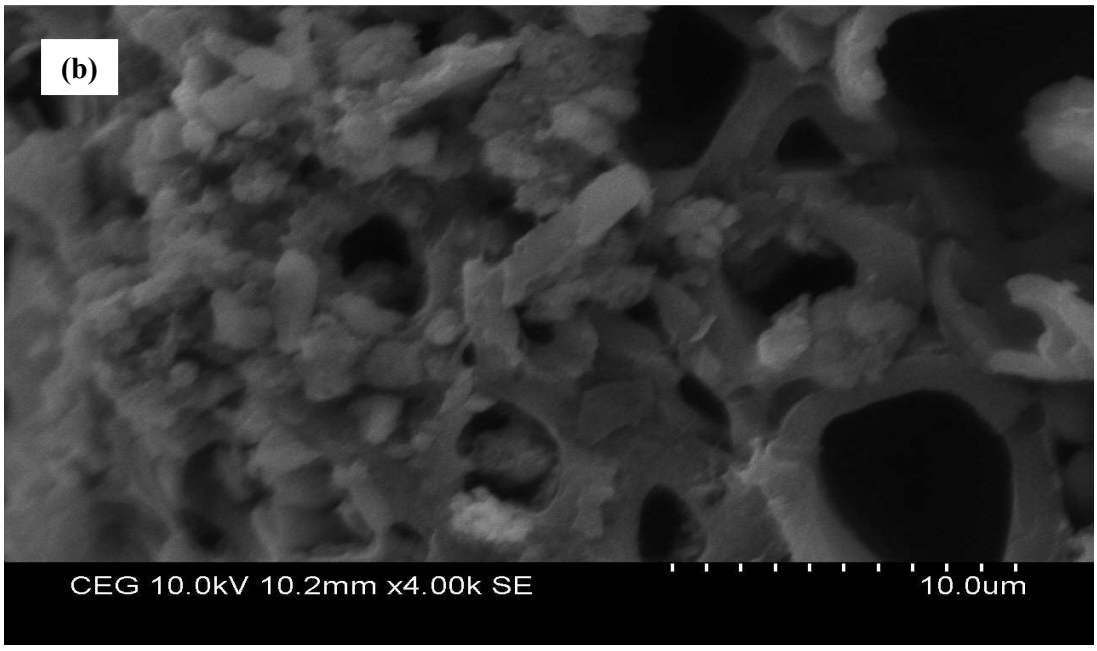

Fig.5 SEM images of (a) FNAC and (b) FNAC-MICE

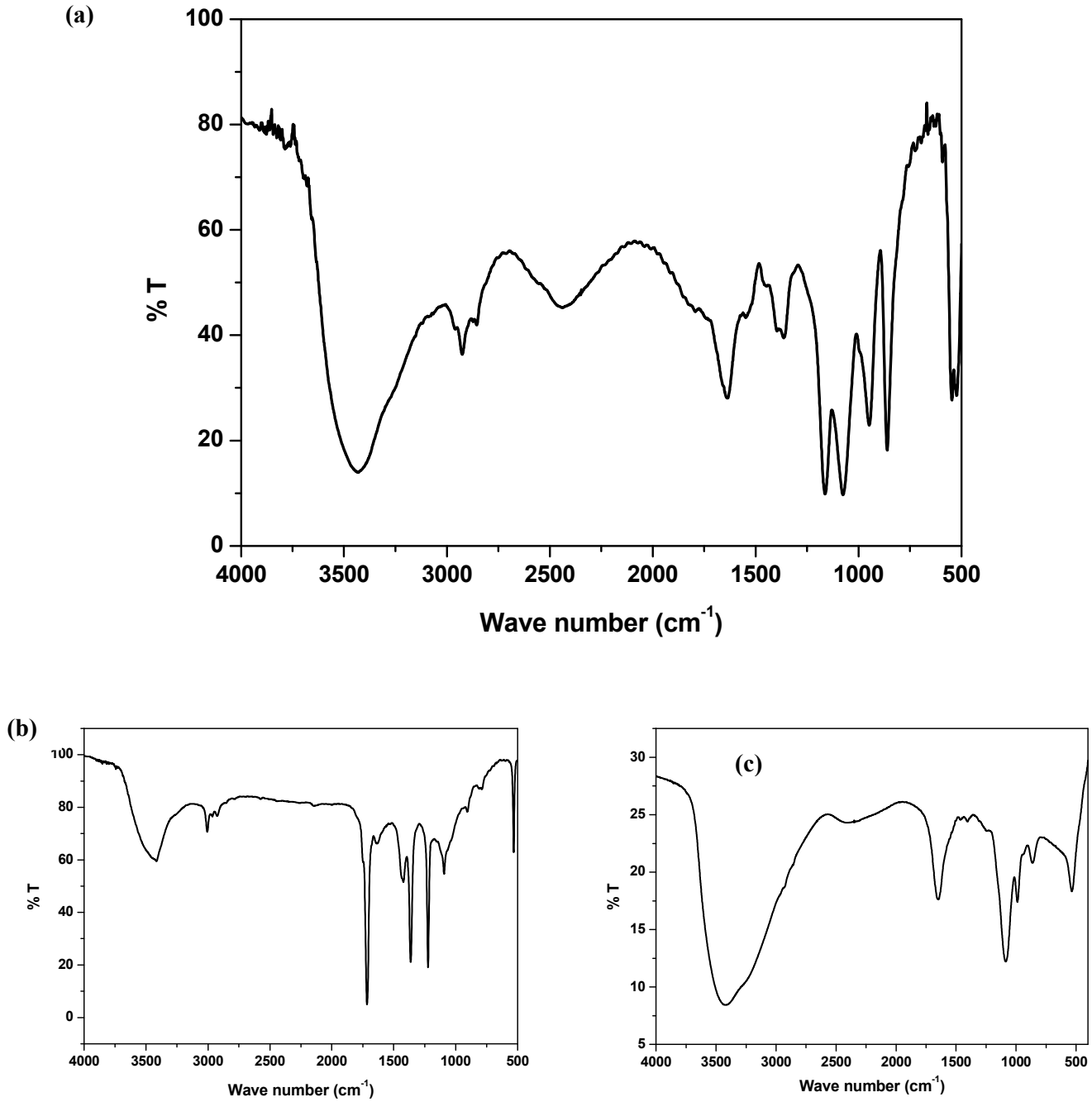

Fig.6 FT-IR spectra of (a) MICE, (b) FNAC and (c) MICE-FNAC

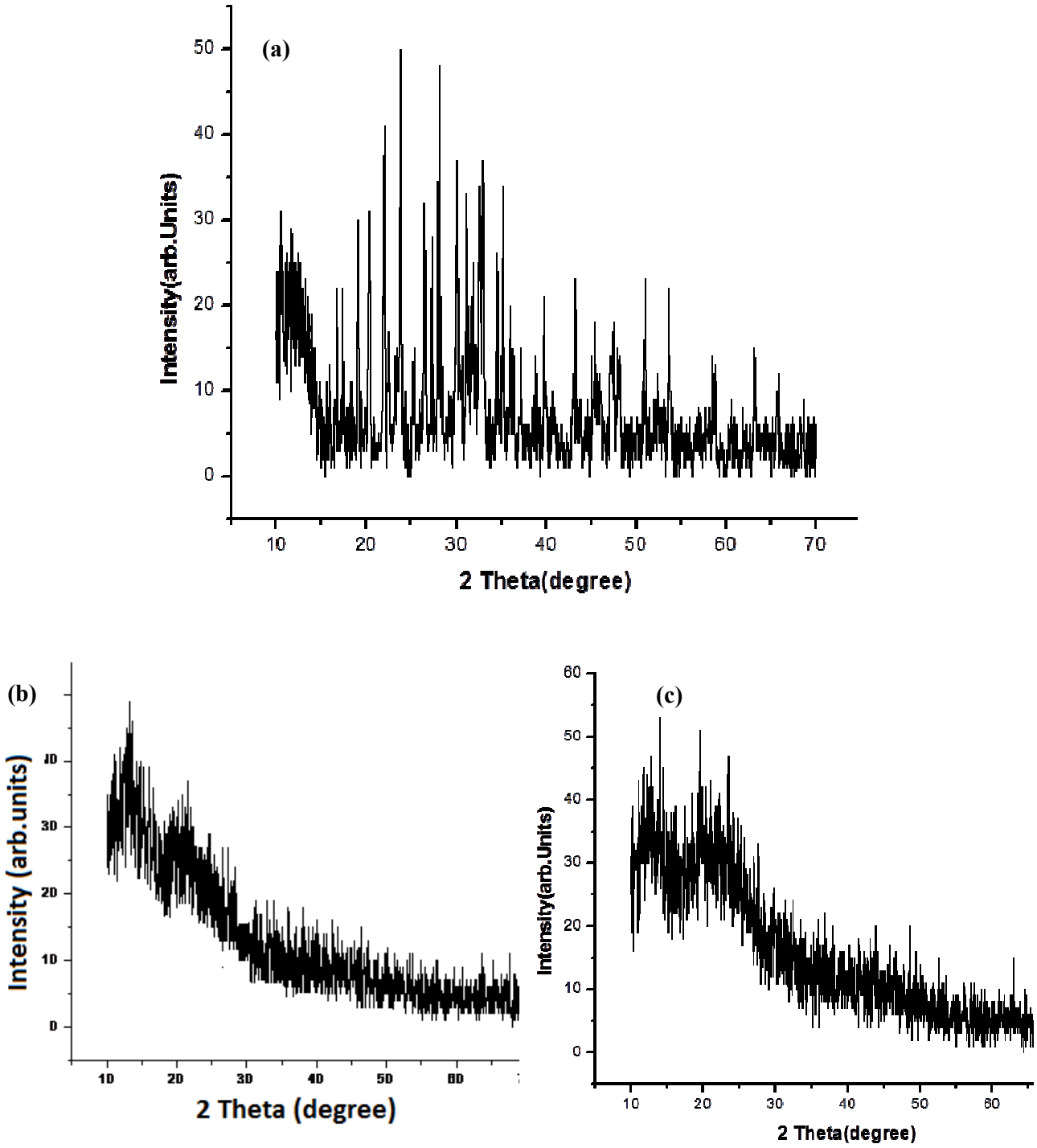

Fig.7 XRD pattern of (a) MICE, (b) FNAC and (c) MICE-FNAC

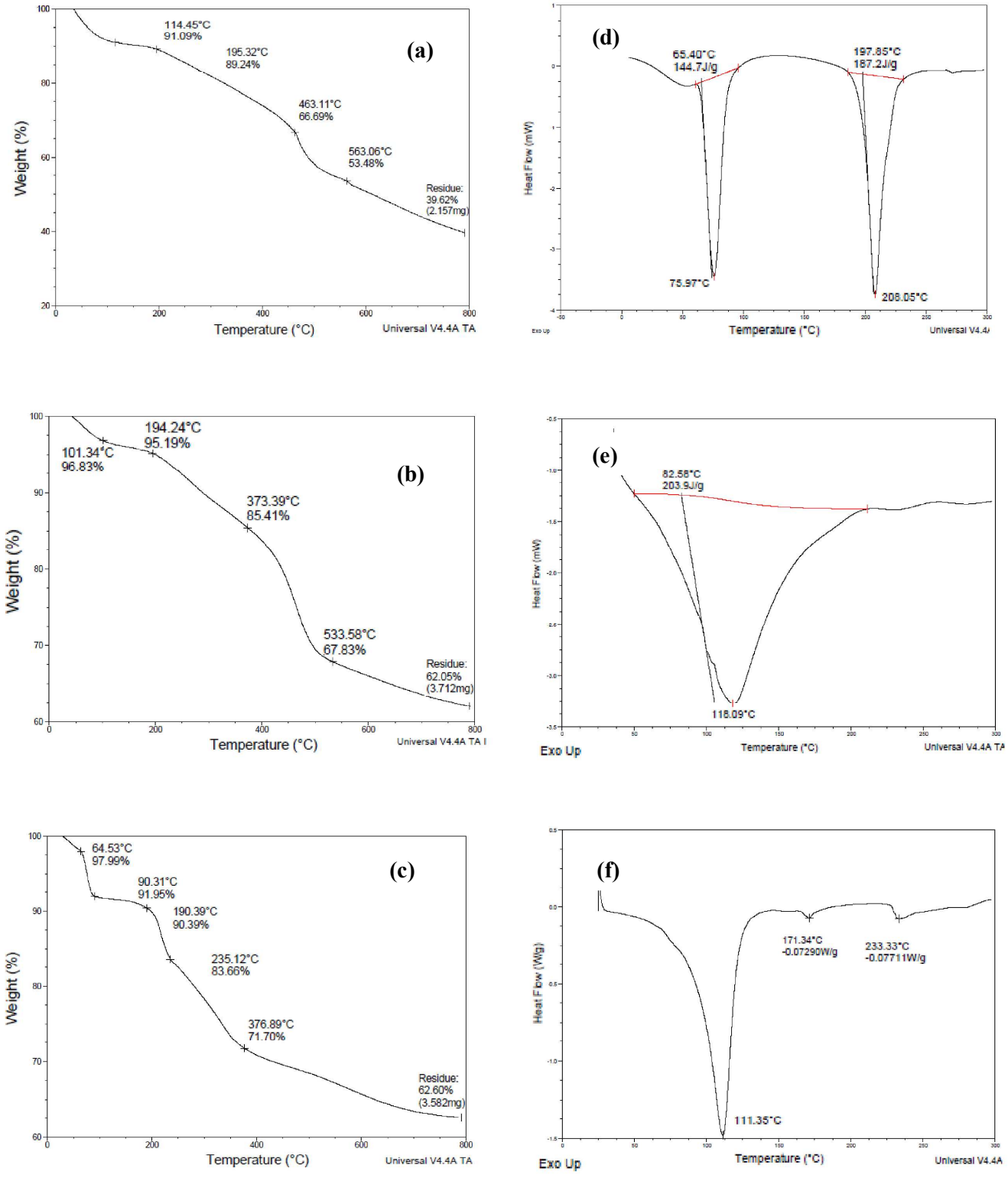

Fig.8 TGA of (a) MICE, (b) FNAC and (c) MICE-FNAC and DSC of (d) MICE, (e) FNAC and (f) MICE FNAC

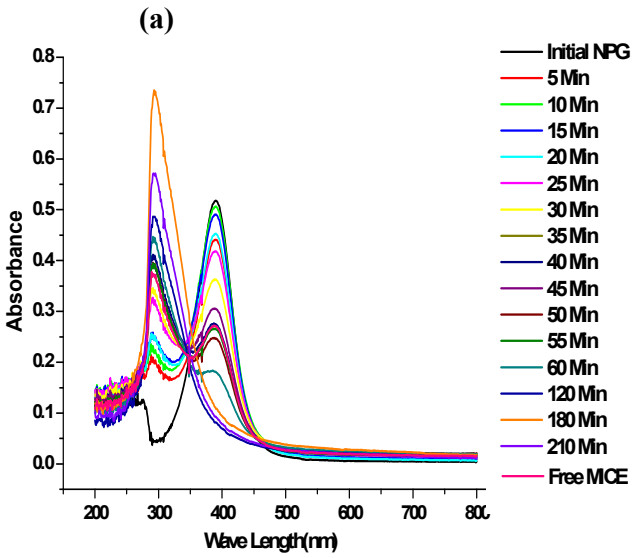

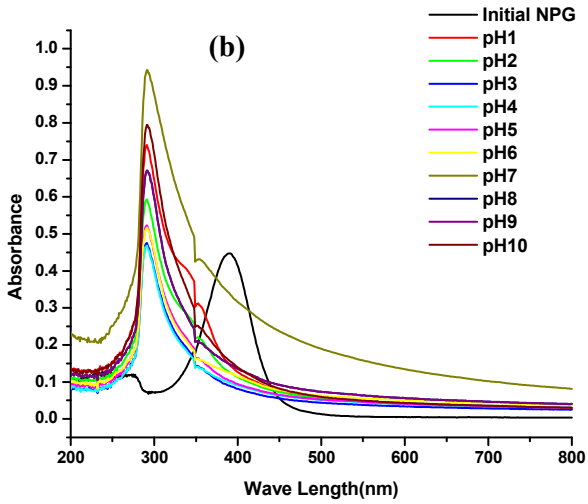

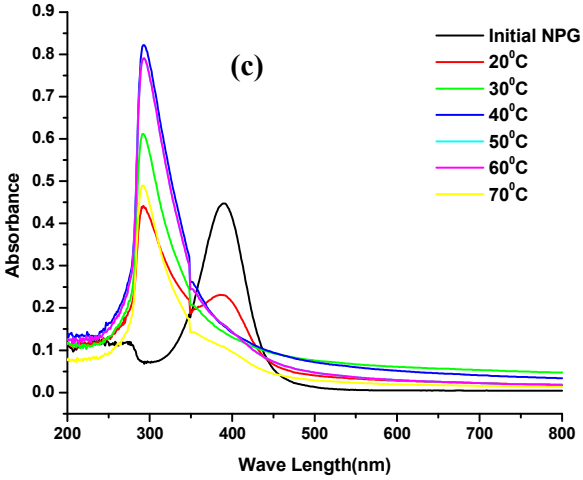

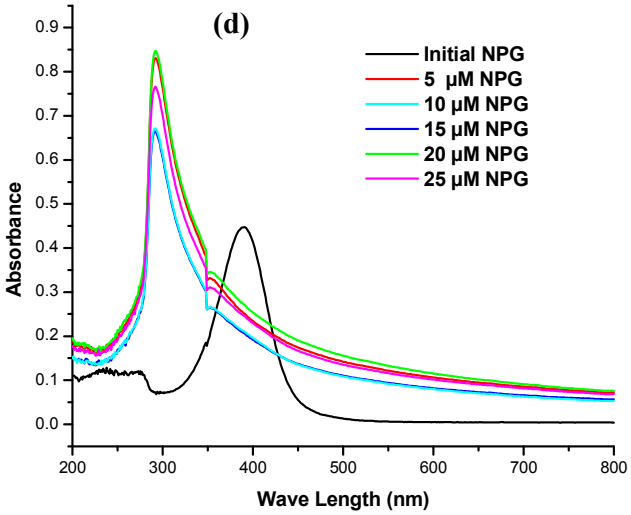

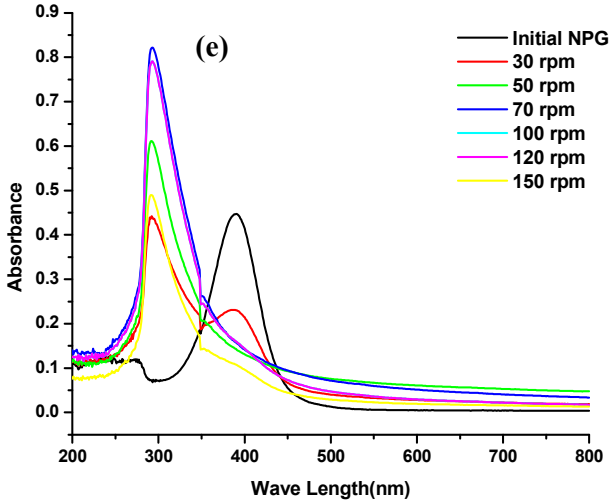

Fig.9 Degradation of NPG using MICE-FNAC (a) Effect of time (Experimental conditions: pH, 7; temperature, 30ºC; initial NPG concentration, 10 µM; agitation speed, 70 rpm), (b) Effect of pH (Experimental conditions: time, 3h; temperature, 30ºC; initial NPG concentration, 10 µM; agitation speed, 70 rpm), (c) Effect of temperature (Experimental conditions: time, 3h; pH, 7; initial NPG concentration, 10 µM; agitation speed, 70 rpm), (d) Effect of initial concentration of NPG (Experimental conditions: time, 3h; pH, 7; temperature, 40ºC; agitation speed, 70 rpm) and (e) Effect of agitation speed (Experimental conditions: time, 3h; pH,7; temperature, 40ºC; initial NPG concentration, 20 µM)

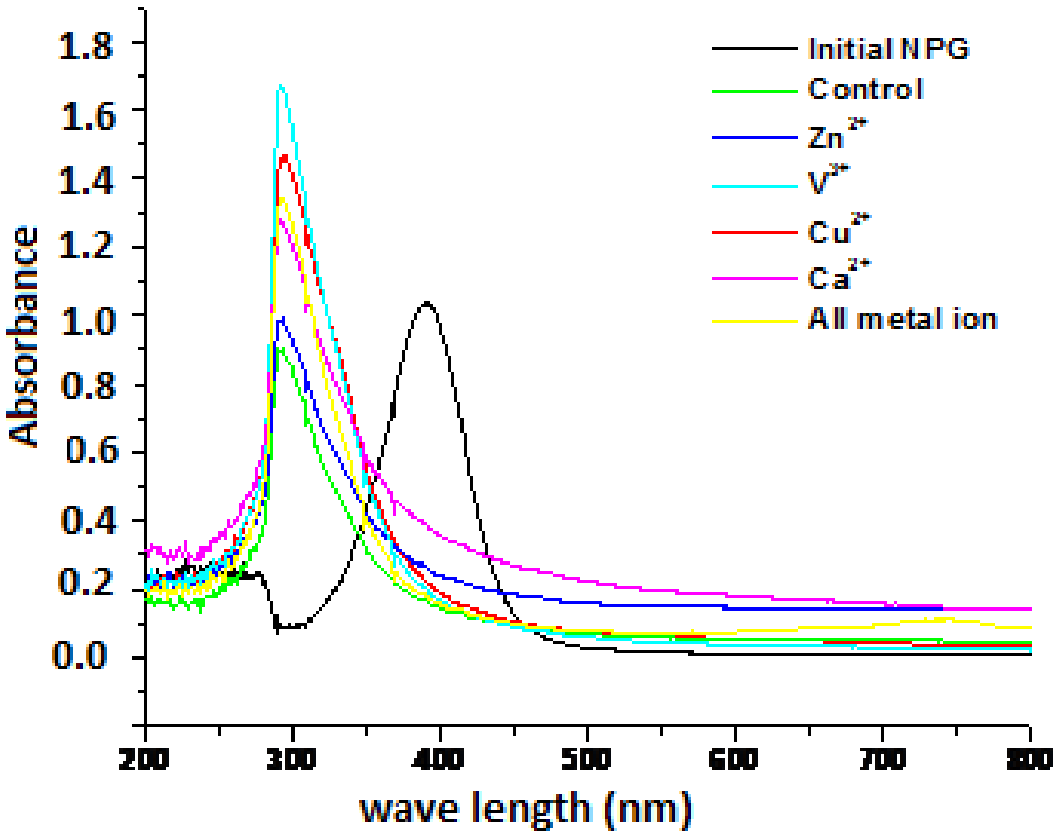

Fig.10 UV-Visible spectra of degradation of NPG by MICE-FNAC in the presence of metal ion enhancers

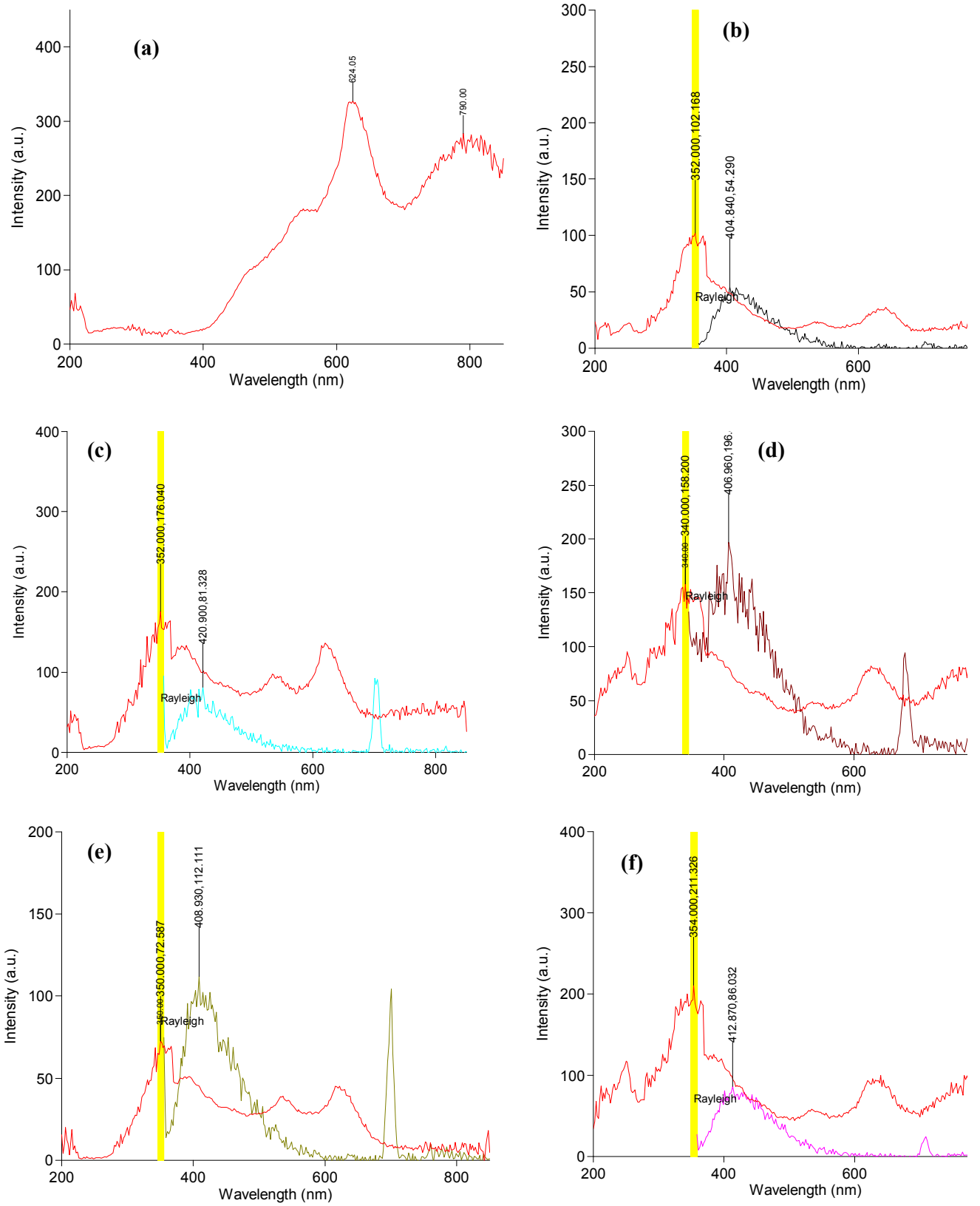

Fig.11 Fluorescence spectra of (a) NPG, (b) NPG degradation using MICE-FNAC in presence of vanadium (c) all metal ions (d) calcium, (e) copper and (f) zinc ion

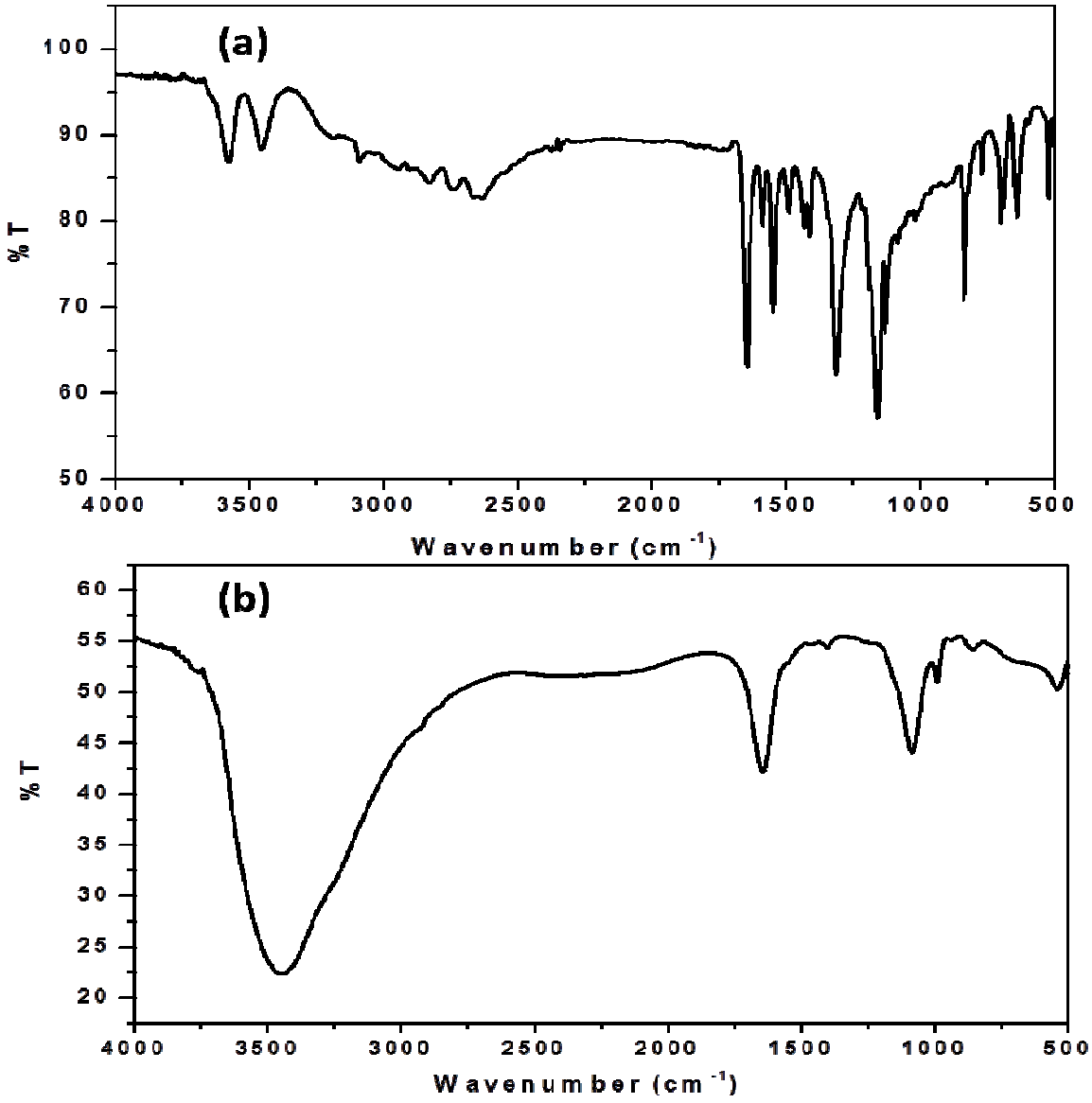

Fig.12 FT-IR spectra of (a) NPG and (b) NPG after treatment with MICE-FNAC

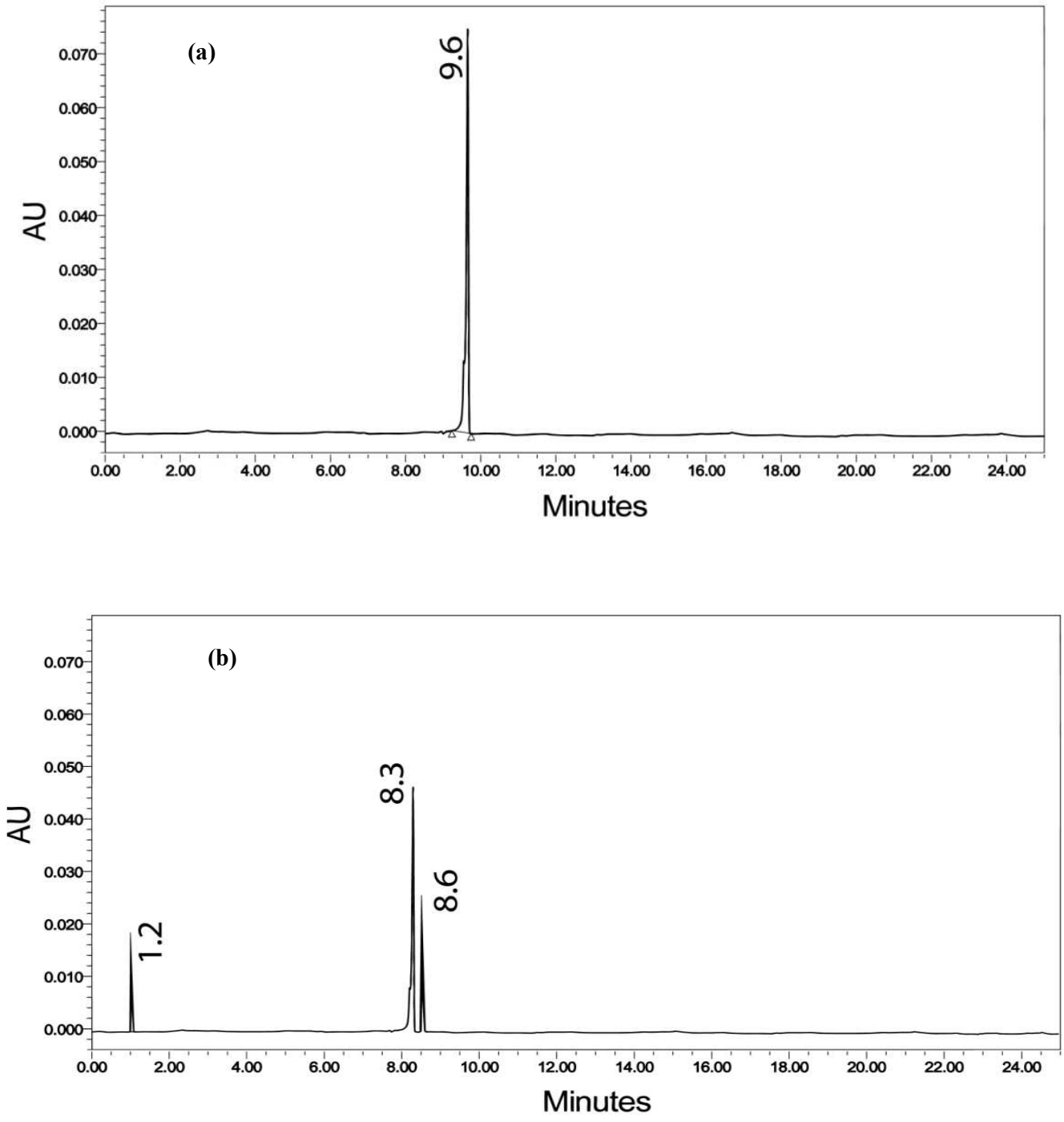

Fig.13 HPLC chromatogram of (a) NPG and (b) NPG after degradation by MICE-FNAC

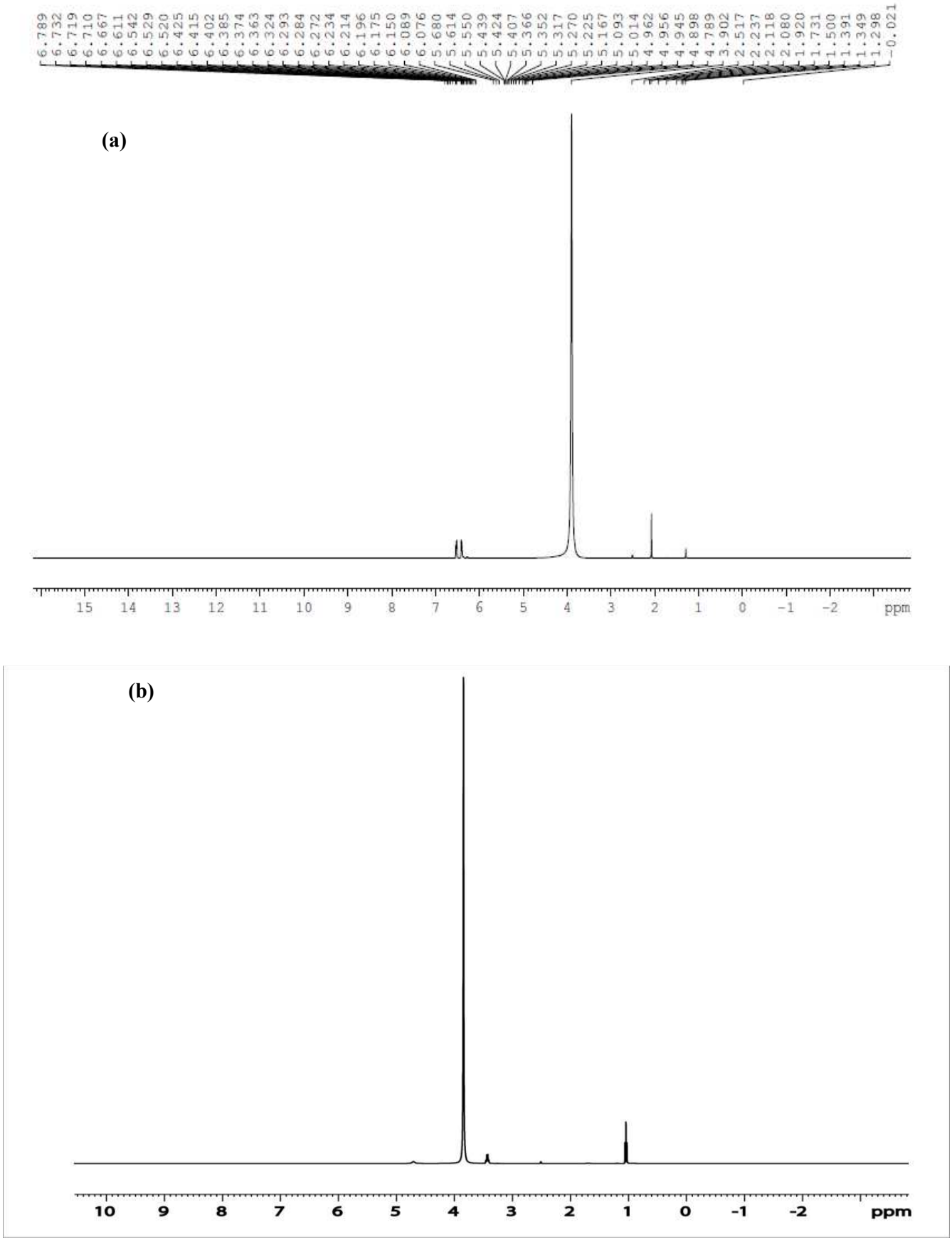

Fig.14 ^{1}H NMR spectra of (a) NPG and (b) NPG after degradation by MICE-FNAC

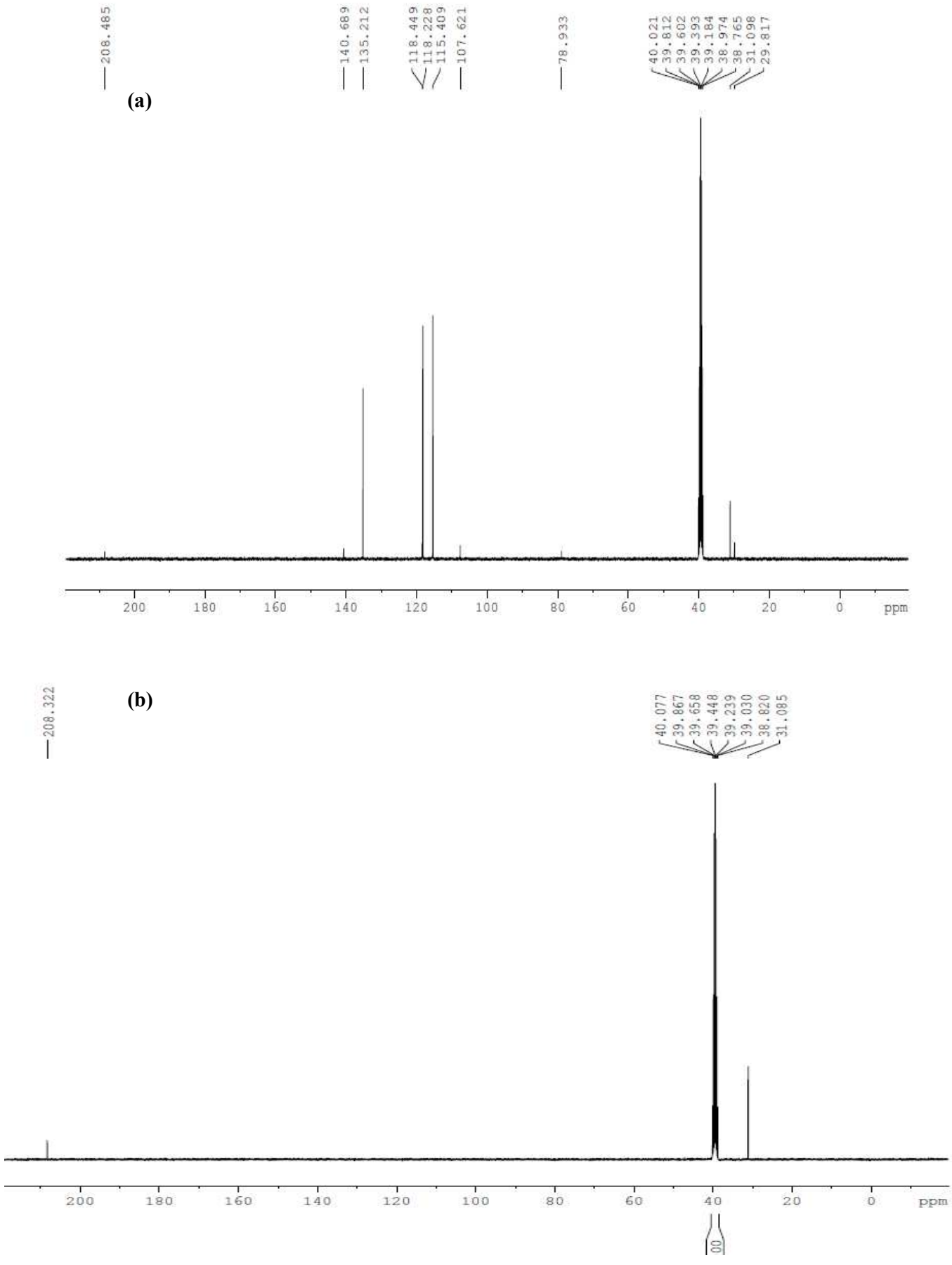

Fig.15 ^{13}C NMR spectra of (a) NPG and (b) NPG after degradation by MICE-FNAC

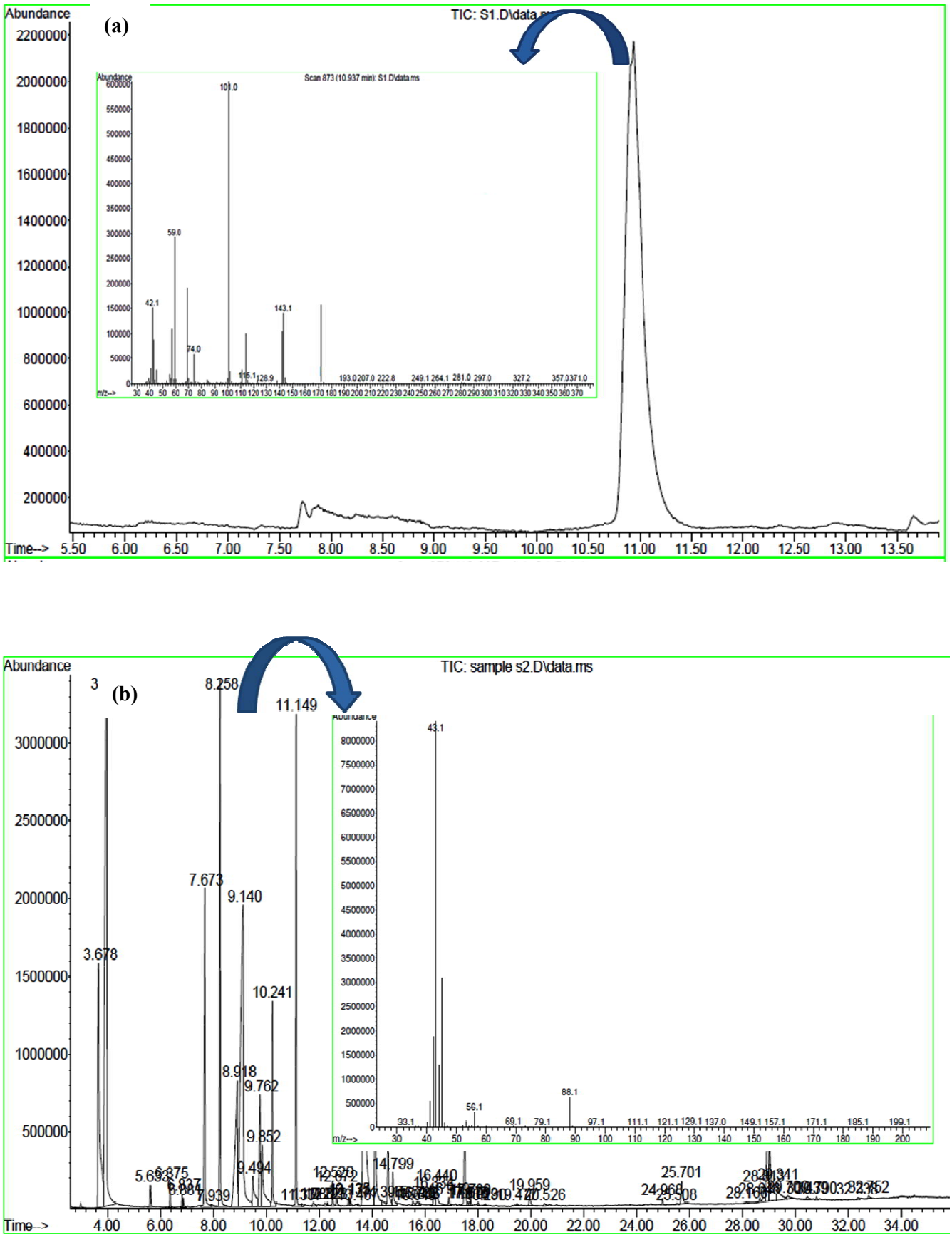

Fig.16 GC-MS spectra of (a) NPG and (b) NPG after degradation by MICE-FNAC

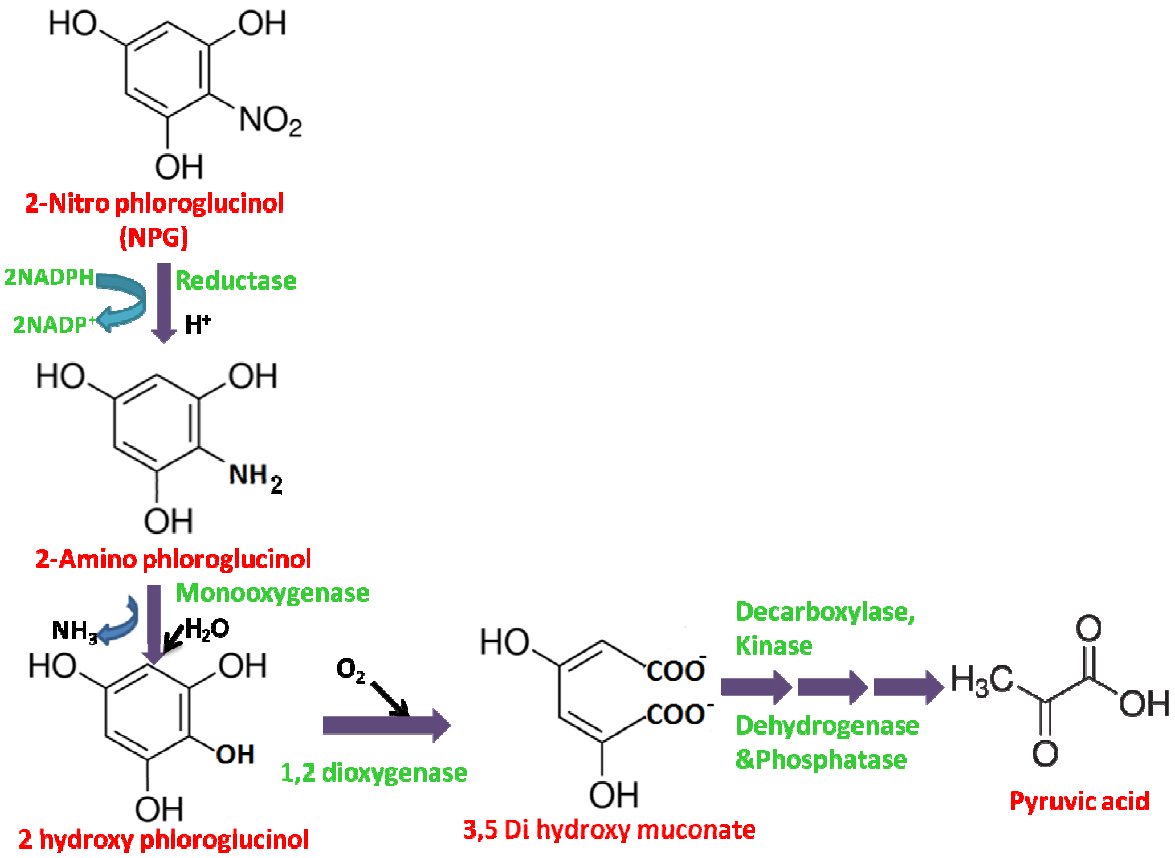

Fig.17 Plausible mechanism of NPG degradation by MICE-FNAC